The Report Committee for Daniel Aaron Woodie certifies that this is the approved version of the following report:

Bayesian Forecasting of Motor Recovery Following Cortical Infarcts

APPROVED BY SUPERVISING COMMITTEE:

Supervisor: _____

Stephen Walker

_____

Theresa Jones

Bayesian Forecasting of Motor Recovery Following Cortical Infarcts

by

Daniel Aaron Woodie, B.S.; M.A.

Report

Presented to the Faculty of the Graduate School of

The University of Texas at Austin

in Partial Fulfillment

of the Requirements

for the Degree of

Master of Science in Statistics

The University of Texas at Austin

December 2015

Abstract

Bayesian Forecasting of Motor Recovery Following Cortical Infarcts

Daniel Aaron Woodie, M.S.Stat.

The University of Texas at Austin, 2015

Supervisor: Stephen Walker

Globally, about 15 million people suffer a stroke each year. Of these affected, about 5 million die and another 6 million are left with long-term disability. The cause of this disability is often due to motor, or muscle, impairments that make everyday tasks like walking or opening a door difficult or even impossible. Improvements in motor function after an injury is due in large part to reorganization of spared neural tissue. To better understand the physiological changes relevant to recovery of motor function, experimental stroke models have been developed. Many studies have focused on neural reorganization as it relates to improvements in motor function following stroke but little has been done to explore the neurovascular remodeling as it relates to these alterations in motor function. To better understand the relationship between restoration of cortical blood flow and improvements in motor function, we first developed a mouse model of stroke that results in recoverable forelimb impairments and then construct statistical models to best link stroke severity and functional outcomes.

Contents

List of Figures

1 Introduction

Globally, about 15 million people suffer a stroke each year. Of these affected, about 5 million die and another 6 million are left with long-term disability (American Heart Association, 2013). The cause of this disability is often due to motor, or muscle, impairments that make everyday tasks like walking or opening a door difficult or even impossible. For these people left with a disability, their recovery phase begins immediately following the initial insult and is characterized by changes in both their function and underlying neural circuitry. Furthermore, improvements in motor function after an injury are due in large part to reorganization of spared neural tissue.

Experimental stroke models using rodents have been especially useful in understanding physiologically changes related to recovery of motor function (Levy et al. 2001; Liepert et al., 2000; Nudo, 2003). For example, it has been shown in mice that stroke to the sensori-motor cortex (SMC) produces forelimb impairments and that the recovery of forelimb impairments is dependent on changes in the cortex surrounding the lesion (Tennant, Jones, 2009). Namely, when a region in the cortex responsible for eliciting movement of the elbow is injured, recovery of elbow function is due to adaptations of uninjured regions of cortex in close proximity. While many neural changes surrounding a lesion have been studied, the influence of local vasculature has been ignored as it relates to functional motor improvements. The central hypothesis of this report is that remodeling the neurovascular architecture contributes to behavioral recovery and cortical reorganization following ischemic insult.

1.1 Stroke Pathology and Epidemiology

Stroke occurs when an area of the brain is deprived of blood (American Heart Association, 2013). This may arise by either a clot that blocks flow (ischemic) or damage to a vessel supplying blood to the brain (hemorrhagic) (American Heart Association, 2013). Whenever an occlusion of this nature occurs, oxygen is no longer delivered to some cells in the brain and the oxygen deprived tissue dies. Dysfunction following a stroke occurs because of damage to functionally specific brain regions. For example, vision problems following stroke coincide with injuries to the visual system and movement problems coincide with injuries to parts of the brain responsible for movement. In the US, stroke is the leading cause of longterm disability (American Heart Association, 2013) and for those that survive a stroke, about 77% exhibit upper extremity dysfunction (Lawrence et al., 2001). These impairments are often a result of damage to the sensorimotor cortex whose neurons descend to the spinal cord (as the corticospinal tract) and connect to neurons which project out to skeletal muscles of the forelimb. To treat stroke which results in disability, clinicians focus largely on rehabilitation because no drugs currently exist to promote functional motor recovery after a stroke.

1.2 Animal Models and Arm Dysfunction

To better understand the causes of various outcomes following human stroke, experimental animal models have been developed. Among these, rodent models have been especially useful for understanding recovery of forelimb function following stroke because lesions to their sensorimotor cortex (SMC) result in tractable upper extremity dysfunction (Bouet et al., 2007; Farr et al., 2002; Tennant, Jones, 2009). Furthermore, from these models we have been able to link the improvements in motor function following a stroke with reorganization of spared neural tissue (Levy et al. 2001; Liepert et al., 2000; Nudo, 2003).

1.3 Activity Dependent Plasticity Following Stroke

Following ischemic lesions, there is a dynamic process where initially cells die in the cortex followed by regenerative events in surviving tissue (Nudo, 2007). This latter process can occur in the tissue surrounding the lesion and contribute to improvements in function (Biernaskie, Corbett, 2007; Castro-Almancos, Borrel, 1995). For example, axonal sprouting and the formation of new synapses in the adjacent tissue after a stroke are linked with motor improvements (Biernaskie, Corbett, 2007; Castro-Almancos, Borrel, 1995). When compared to spontaneous recovery, or recovery without interventions, training the impaired forelimb after a stroke promotes adaptive changes in the tissue near the lesion in the motor cortex and improves forelimb function

in rodents (Biernaskie, Corbett, 2007; Biernaskie, Chernenko, Corbett, 2004). Many studies focus on understanding the neuroanatomical changes which contribute to this adaptive plasticity but few are focused on the contributions of vascular changes. The irony in this is that stroke is a traumatic event caused by a disruption in vasculature (American Heart Association, 2013), however, most work has not focused on how vascular reorganization may contribute to cortical plasticity and improvements in forelimb function. That is, while reorganization of the cortex is neural activity-dependent (Liepert et al., 2000; Nudo, 2003), changes following an ischemic injury also indicate the dependence of blood flow – thus, there is likely a dependence between adaptive plasticity and restoration of blood flow.

1.4 Vascular Dependence of Neural Plasticity

Blood flow is closely linked to changes in the brain. For example, many inferences drawn from brain imaging studies rely on blood flow being increased in regions of heightened neural activity (i.e., activation-flow coupling) (Ances et al., 1999). Additionally, activities such as running or exercise can induce angiogenesis in the brain (Swain et al., 2003). While stroke immediately results in damaged blood vessels becoming more damaged, there is also a counter to this damage where angiogenesis and shunting of collateral blood vessels occurs (Wei et al., 2001). This process of vascular remodeling following an injury results in the creation of many new blood vessels, some transient and leaky, and the blood flow restored to certain regions is likely to depend

on the integrity of these new vessels as they mature (Dirnagl, Iadecola, Moskowitz, 1999). Overall, this pattern of re-establishing blood flow to damaged regions has been connected with the formation, elimination, and stabilization of dendritic spines (Mostany et al., 2010). The time-course of this vascular process has not been studied in tandem with recovery of motor function following a stroke.

1.5 *In vivo* Imaging and Mouse Models of Stroke

To study the temporal link between recovery of blood flow and recovery of forelimb function following a stroke, we settled on developing a rodent model that receives a focal infarct to the SMC as it has been shown to reliably induce upper extremity impairments (Tennant, Jones, 2009). To repeatedly image cortical blood flow, we installed a cranial window over the SMC (See Figure 1) (Holmaat et al., 2009). This approach allowed us to combine *in vivo* imaging with sensitive tests for forelimb motor function (Kazmi et al., 2013). With using *in vivo* imaging, the mouse as a model has been more extensively developed because of it's genetic malleability which can be used for fine-tuned imaging (namely for their thin skulls and transgenic capabilities) (Mostany, Portera-Cailliau, 2008; Yang et al., 2010; Holmaat et al., 2009; Svoboda et al., 1997; Tomita et al., 2005; Kazmi et al., 2013). We used a non-invasive approach to induce the lesion which involved a light and a light activated solution which creates a thrombus (See Figure 1) (Brown et al., 2007; Brown et al., 2009). Installing cranial windows over the SMC allowed for both repeated imaging of cortical blood flow and

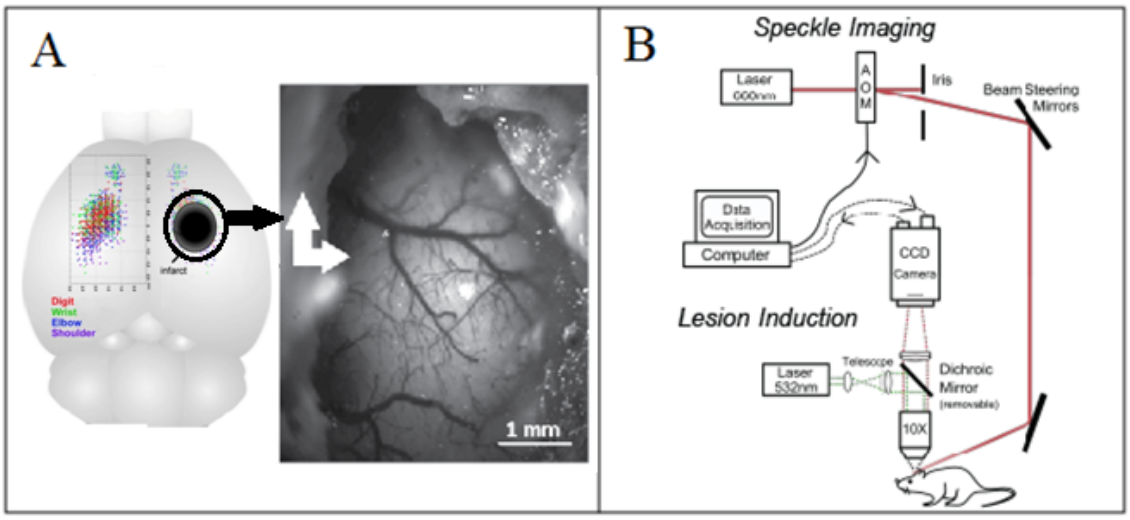

Figure 1: A: Mice will have a cranial window installed over their sensorimotor cortex for lesion induction and repeated imaging. B: Lesion induction and cortical blood flow imaging. Ischemic lesions will be created by injecting Rose Bengal and then focusing a green laser through a 10X objective for 15 minutes. Controls received injections of saline instead of Rose Bengal. The imaging setup is a variation on speckle imaging called MESI which allows for *in vivo* measurements of cortical blood flow rates.

the precise creation of lesions (Kazmi et al., 2013). This was key to developing an injury model with motor deficits and temporally linking the restoration of blood flow changes. To assess upper extremity function, we used the pasta matrix reaching task (PMRT) because this metric has been established as a reliable metric for skilled forelimb function in mice.

1.6 Current Study

The primary motivation for this study is that stroke disables such a large population but little work has been done to determine the extent to which the local vasculature

influences functional recovery. Fortunately, recent developments in rodent models (e.g. *in vivo* imaging), which have allowed for a much more granular understanding of adaptive plasticity following stroke, make the temporal exploration of blood flow recovery possible. This study addressed this shortcoming by using behavioral manipulations with *in vivo* imaging to determine the relationship between motor improvements and recovery of blood flow in peri-infarct cortex. By observing the time course of cortical blood flow restoration in tandem with the recovery of skilled forelimb function following a unilateral infarct to the SMC, we aimed to establish the relationship between neuro-anatomically relevant recovery of blood flow with improvements in motor function. In so doing, this model will improve the direction of experimental models of chronic stroke and inform clinical treatment approaches.

To better understand the relationship between restoration of cortical blood flow and improvements in motor function, we developed a mouse model of stroke to the SMC that results in recoverable forelimb dysfunction and can be repeatedly imaged in vivo. To allow for repeated imaging, a portion of the skull over the SMC was replaced with a thin glass sheet. After two weeks recovery from this window installation, mice then either received ischemic lesions to their SMC ($n = 7$) or vehicle procedures ($n = 7$). The lesion was created by injecting a solution that reacts with a green light (Rose Bengal) and then focusing a green light over the SMC through the cranial window. This sustained illumination results in a blood clot when Rose Bengal is in circulation, and when the green light is focused over neural tissue – an ischemic

lesion results. Vehicle animals received the same procedures except saline was injected (diluent) instead of Rose Bengal. After lesions were created, mice were then allowed 20 days of recovery and were tested on forelimb function in tandem with measuring cortical blood flow at Days 3, 5, 10, and 20. Forelimb function was measured using the pasta matrix reaching task (PMRT) and cortical blood flow was quantified using multi-exposure speckle imaging (MESI).

We expected that cortical infarcts will result in spontaneous improvements in cortical blood flow that will temporally relate with improvements in skilled forelimb function. We expected blood flow recovery to be more limited in the infarct core and for blood flow recovery to increase spatially moving away from the core. Furthermore, regions with the greatest recovery of blood flow corresponded to more normal vessel densities and to greater surviving forelimb movement representation area. Also, as expected, the magnitude of the recovery of blood flow recovery in surviving forelimb regions was predictive of improvements in skilled forelimb function.

While this study was experimental, the relationship that we are modeling is not, in fact, addressing causation. To determine the extent to which the restoration of cortical blood flow causes recovery of forelimb motor function, further experiments would need to be conducted which modulate vascular remodeling following an infarct. That is, following a lesion new blood vessels are created and un-damaged vessels are re-purposed to supply flow to the infarct core and penumbra. Both of these processes would need to be blocked to determine the exact influence of vascular remodeling as

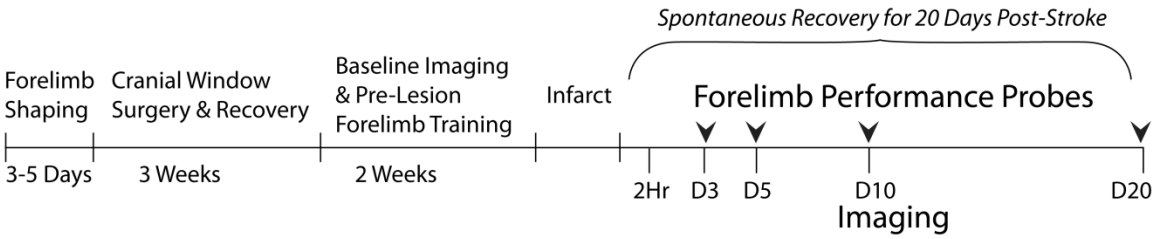

Figure 2: Experimental design. After determining their preferred for reaching forelimb using the PMRT, mice then had a cranial window installed over the contralateral region of their motor cortex. Following a 3 week recovery period from the cranial window surgery, mice then received 2 weeks of skilled forelimb training using the PMRT. In this 2 week period mice also received 3 baseline imaging sessions using MESI. At the end of this period, mice either received a photothrombotic lesion or vehicle procedures followed by 20 days of spontaneous recovery with behavioral and impaging probes at days 3, 5, 10, and 20. At day 20, mice were perfused and their tissues harvested for post-mortem histology.

it relates to improvements in motor function following a lesion.

2 Methods

2.1 Design Overview

Three weeks after window installation, mice were trained with the dominant forelimb on the pasta matrix reaching task (PMRT) until they could retrieve at least 7 pasta pieces (~70% of the maximum) per training session (Tennant, Jones, 2009; Kerr et al., 2013). During this pre-stroke training period, mice also underwent a series of 3 baseline imaging sessions, spaced at least 3 days apart, to establish basal blood flow rates (Kazmi et al., 2013). After reaching the criteria on the PMRT, a photothrombotic lesion to the caudal forelimb area (CFA) of the motor cortex contralateral to the dominant forelimb will be induced in half the mice, so that the trained forelimb becomes the paretic forelimb. Following a 3 week recovery period from the cranial window surgery, mice then received 2 weeks of skilled forelimb training using the PMRT. In this 2 week period mice also received 3 baseline imaging sessions using MESI. At the end of this period, mice either received a photothrombotic lesion or vehicle procedures followed by 20 days of spontaneous recovery with behavioral and impaging probes at days 3, 5, 10, and 20. At day 20, mice were perfused and their tissues harvested for post-mortem histology. At the conclusion of the experiment, animals were overdosed with sodium pentobarbital (150 mg/kg) and transcardially perfused with 0.1 M phosphate buffer followed by 4% paraformaldehyde in the same buffer.

2.2 Subjects

14 male and female mice were group housed (3 or 4 to a cage) on a 12:12 light/dark cycle in the Animal Resource Center. These mice received weekly cage supplement (e.g. bedding, PVC pipes, and wooden toys). At the time of the experiment, mice were placed on a restrictive diet (dropping to no less than 90% of their initial body weight) and kept on this diet for the duration of the experiment. After determining limb dominance for reaching (left or right), all mice had cranial windows installed over the contralateral SMC. The mice were randomly assigned to receive lesion or vehicle procedures. For the MESI data, three mice were removed from the vehicle condition because their window became cloudy and their cortex was not visible. While these mice were not repeatedly imaged, they still were anesthetized at the same time points to correct for any influence that repeated anesthesia may have had on behavioral results. All procedures with the mice were approved by the University of Texas Institutional Care and Use Committee, an AAALAC accredited program.

2.3 Pasta Matrix Reaching Task

Mice were both trained and tested on the PMRT. To determine their dominant forelimb, mice were placed in a plexiglass chamber and allowed to reach for Capellini pasta pieces arranged vertically outside of the chamber. Mice were able to reach and retrieve pasta through a slit in the plexiglass chamber. The dominant forelimb

was determined by counting reach attempts for pasta. If a mouse made at least 20 reach attempts and 60% or greater of these were with a single forelimb then it was determined to be their dominant forelimb. After installation of the cranial window, mice then received 14 successive days of forelimb training in which they were placed in the plexiglass chamber with pasta now arranged diagonal from their preferred for reaching forelimb through the slit. As such, mice were only able to successfully retrieve pasta using their dominant forelimb. Mice reached 100 times for pasta during each day of training and reach performance was calculated as no. of pieces broken/ no. of reach attempts (100). After photo-thrombotic lesions or vehicle procedures, mice were assessed with their dominant forelimb at days 3, 5, 10, and 20 at 24 hours after each imaging session.

2.4 Multi-Exposure Speckle Imaging

Cortical blood flow was assayed with MESI (variation on speckle imaging which provides absolute flow rates for cortical blood flow). Before mice received stroke or vehicle procedures, they underwent a series of 3 baseline imaging sessions, spaced at least 3 days apart, to establish basal blood flow rates. Mice then had their cortical blood flow measured 2h, and 3, 5, 10, and 20 days after lesion induction. Images from multiple time points can be compared within and between subjects. These images are generated by first determining the speckle contrast value (standard deviation/mean image intensity) for a 5x5 pixel cluster. Images were then acquired across 15 different

exposure times and the information from each exposure time integrated to provide the final MESI frame (Kazmi et al., 2013). MESI imaging was performed under isoflurane anesthesia (to maintain immobility). To correct for any influence of anesthetic plane, physiological parameters were continuously monitored (with MouseOx) and isoflurane levels adjusted such that heart rate and blood oxygenation levels varied no more than 10% across all imaging sessions.

2.5 Surgrical Procedures

2.5.1 Cranial Window Installations

Following determination of their preferred for reaching forelimb, mice had a cranial window installed over their contralateral region of their motor cortex. Mice were first anesthestized with 120 mg/kg ketamine and 9 mg/kg xylazine and a circular craniotomy (~3 mm in diameter) performed. Photos of the skull, window and underlying vascular patterns are taken to enable later placement of the lesion based on coordinates relative to skull landmarks. A circular glass coverslip was then placed over the opening and sealed with cyanoacrylate. Mice were then allowed three weeks of recovery before beginning any other experimental procedures and received weekly injections of carprofen.

2.5.2 Photothrombotic Lesions

To create a photothrombotic lesion, mice were anesthetized with 2% isoflurane and were maintained with 1% isoflurane. The mice then received Rose Bengal (.15 mg/ml i.p) and, 3 minutes following the injection, a green laser (35 mW) was focused over the forelimb area of the motor cortex through a 5X objective (.1 NA) for 15 min. The region selected as the forelimb area was estimated by images of the craniotomy taken at the time of cranial window installation. These images had both skull and cortical vascular landmarks which allowed for accurate approximation of the CFA. Animals that received vehicle procedures had identical experiences but were injected with saline (solvent for Rose Bengal) instead of Rose Bengal.

3 Data

3.1 Data Not Included

At the start of this study, 14 mice were included but 3 were removed because they developed an inflammatory response where the cranial window was installed which impeded visibility needed for accurate estimates of cortical blood flow. While these mice were not included in the models, they were taken to completion of the study and received otherwise identical experiences to those mice in the analyses below. Furthermore, although this shortcoming exists in the data used to construct our models, there is data currently being collected which would allow for further testing of the models built herein.

3.2 Quantification of Stroke Severity

For each mouse, a series of baseline MESI files were acquired prior to lesion induction. We acquired multiple images because of fluctuations in breathing and heart rate patterns under anesthesia which have been shown to influence measurements of cortical blood flow. To quantify cortical blood flow, images acquired through MESI were used because they provide information on absolute blood flow rate. Each imaging frame is a 400 x 600 pixel frame corresponding to about 4 x 6 mm. This frame was deconstructed from a matrix to a vector and the 90% trimmed mean was calculated for each image. To calculate blood flow change from baseline, each image was compared

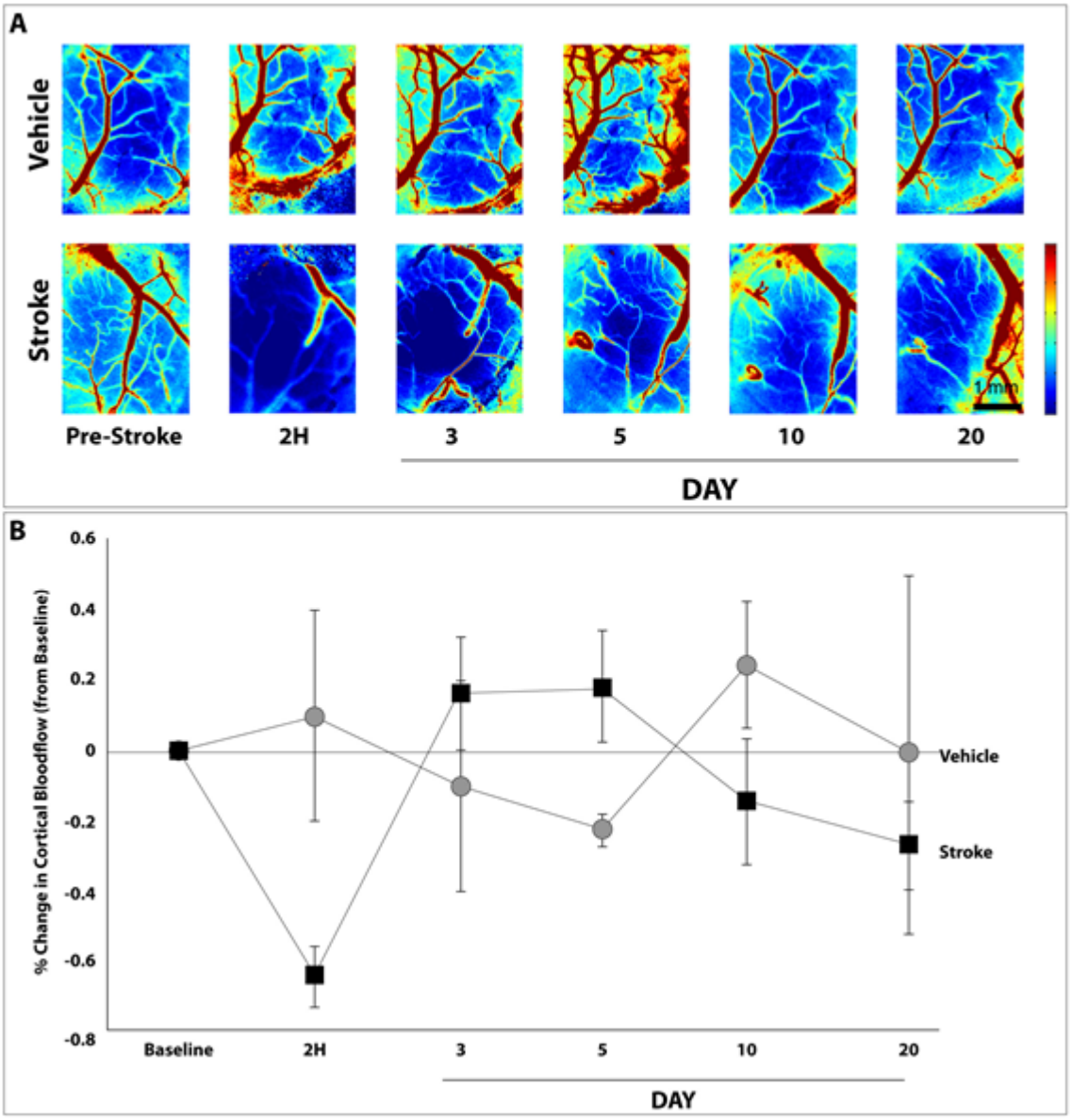

Figure 3: A. After 3 baseline imaging session spaced over 14 days, all mice received either photothrombotic lesions or sham procedures. All animals were then imaged 2 hours, 3 days, 5 days, 10 days, and 20 days following the lesions. B. Ninety percent trimmed means of the MESI frames were computed and change calculated from heart-rate matched baseline frames. This data show that there was a significant reduction in cortical blood flow 2 hours after the lesion compared to vehicle controls. Furthermore, this effect was gone by three days after the lesion and continued to the end point of the study.

with the pre-stroke baseline image that had the closest recordings from the MouseOx. Stroke severity was calculated as a percent reduction in flow 2 hours following lesion induction compared with a baseline measurement of blood flow or

$$\frac{Blood\ Flow_{2hrpost} - Blood\ flow_{pre}}{Blood\ Flow_{pre}}$$

This value calculated was later used in the statistical models as x_i where i represents the ith mouse.

3.3 Forelimb Performance Data

For 14 days prior to lesion induction and at days 3, 5, 10, and 20, mice performed the PMRT. Forelimb performance was measured by number of pasta pieces broken by each mouse in the PMRT. To calculate the performance at time t for mouse i, the number of pieces broken at time t was subtracted from the maximum number of pasta pieces broken before the lesion and divided by the maximum number of pasta pieces broken before the lesion or:

$$Y_{i,j} = \frac{\#\ of\ pasta\ pieces\ broken\ t\ days\ after\ lesion\ by\ mouse\ i}{max\ \#\ of\ pasta\ pieces\ broken\ before\ lesion\ by\ mouse\ i}$$

. where $Y \in \{0, 1\}$ with values closer to 0 representing more substantial impairments and those closer to 1 representing performance on par with the best performance before a lesion.

4 Statistical Modeling and Estimation

This section describes approaches for 1) linear and 2) non-linear modeling of cortical blood flow and motor function following ischemic cortical infarcts. With linear modeling, repeated measures analysis of variance on both forelimb function and cortical blood flow was used. From there the correlation between these two variables was calculated. With non-linear modeling, the focus was instead on developing a form for our model to follow. Once the form was established, a few specific models were then vetted to determine the best fit. Upon determining the best non-linear model, the model was then adapted so that each subject could have their own parameter estimates. This approach decreases the overall variance of the model but makes inference on the parameter estimates questionable at best. To improve inferences on the parameters, a Bayesian approach was then taken where priors were attached to each of the parameters in the model which allowed for a more easily interpretable posterior distributions. All analyses were conducted using R.

4.1 Linear Modeling

The *in vivo* measurements of cortical blood flow were assessed across time points using repeated measures analysis of variance (ANOVA) to determine temporal specifics of blood flow gain and loss. Forelimb performance was analyzed using repeated measures ANOVA as well to explore the effect of Stroke, Day, and Stroke by Day

interaction. Simple effects were assessed using independent t-tests. Correlation models were constructed to determine the linear relationship between cortical blood flow changes and functional motor performance.

4.1.1 Reaching Performance

Following the lesion, mice that received a photothrombotic lesion displayed significantly reduced forelimb performance compared to controls for up to 10 days (Figure 4). To establish this, we ran a repeated measures ANOVA with a treatment by day interaction ($F(4, 36) = 3.908, p = .01$). To investigate the simple effects of the changes in baseline motor performance at days 3, 5, 10, and 20 we performed independent t-tests. These independent t-tests produced were significant for days 3 ($t(4.457) = -2.831, p = .021$) and 5 ($t(8.739) = -2.588, p = .042$). The differences disappeared by day 10 ($t(5.813) = .093, p = .535$) and continued through day 20 ($t(7.840) = -.258, p = .402$).

4.1.2 Cortical Blood Flow

Mice that received a photothrombotic lesion displayed a significant reduction in blood flow 2 hours following the stroke but this effect was no longer present 3 days following the stroke and continued for the duration of the experiment (Figure 3). In repeated measures ANOVA there was a significant between groups and time interaction in the change from baseline cortical blood flow ($F(4, 32) = 4.781, p = .004$). We used independent t-tests at each of the time points following stroke but the only significant

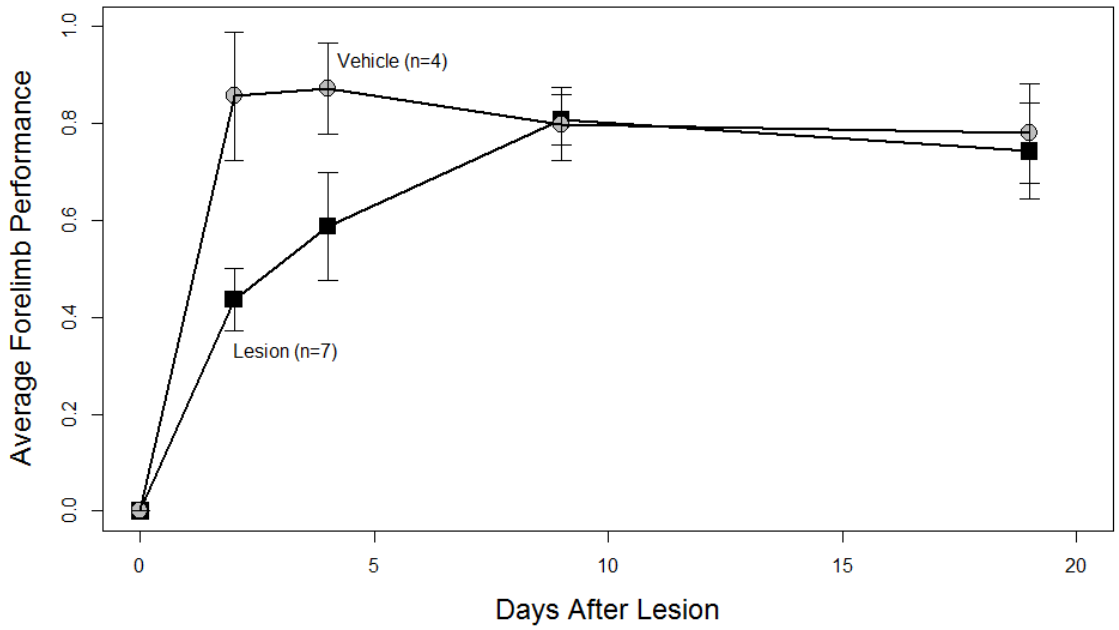

Figure 4: Forelimb reaching performance. All mice received 14 days of forelimb training before receiving stroke or vehicle procedures (lesion induction). The measurement at time = 0 was set to 0 for each mouse and all following measurements are presented as a percentage of the max from the 14 days of pre-lesion training. Mice that received the lesion procedures displayed significantly decreased performance compared to sham-operated controls for days 3 and 5 after ($p<.05$). This effect was ablated by day 10 and continued to day 20 ($p>.05$). Data are displayed as mean ± SEM.

difference was that at 2 hours ($t(9) = -2.732, p = .023$).

4.1.3 Cortical Blood Flow and Behavior Correlations

Correlations between cortical blood flow and forelimb performance were calculated for mice that received lesions. As mice that did not receive lesions were not expected to display fluctuations in cortical blood flow that reflected forelimb performance, they were not included in these calculations. Behavioral performance following the lesion correlated most strongly with stroke severity 3 days following the lesion ($r = .97, p < .001$) but also showed strong correlations at days 10 ($r = .78, p = .038$) and 20 ($r = .775, p = .041$). Oddly, behavioral performance was not correlated with stroke severity at 5 days following the lesion ($r = -.201, p = .665$).

4.2 Non-Linear Modeling

From this data, models for recovery of forelimb function as indexed by Y_i at time t_j which depend on stroke severity x_i were constructed which follow the form of the data when plotting the overall average of the Y_i's across time t_j's (see Figure 6). Additionally, when separating the two groups (those that received a photothrombotic lesion and those that received control procedures) a pattern becomes apparent (see Figure 7) where the group that received a lesion approaches a full recovery slower than the group that received vehicle procedures. As such, we'd want the part of our model that is informed by the lesion severity to influence the part of the function

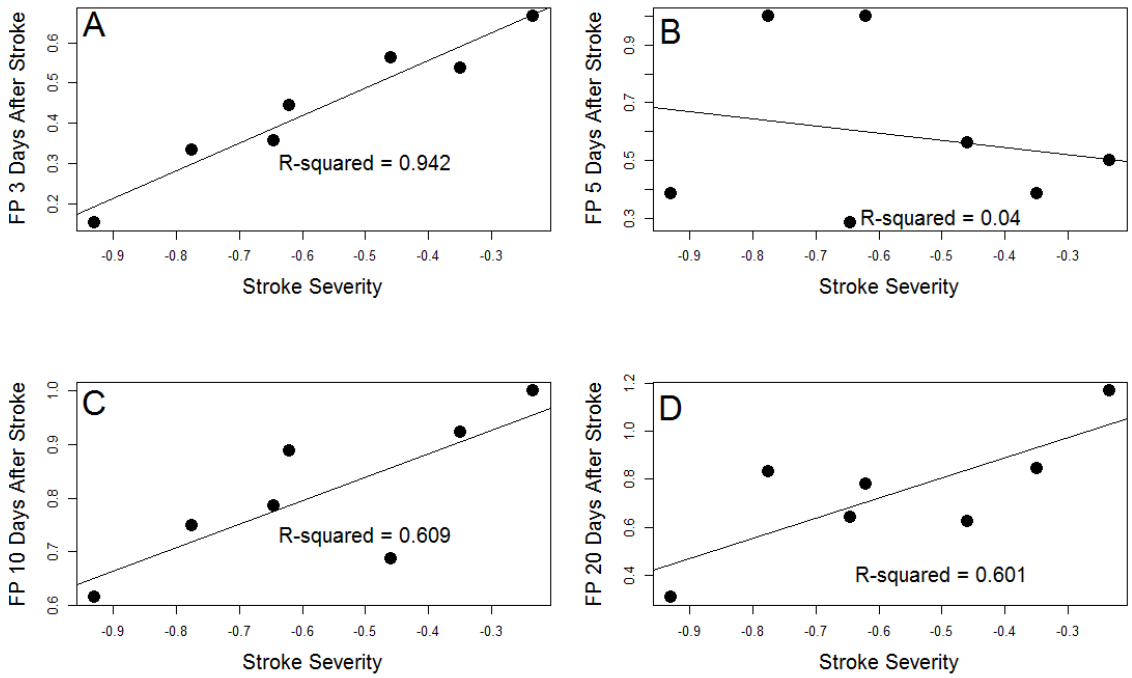

Figure 5: Correlations between cortical blood flow and forelimb performance. A: Forelimb performance three days after the lesion is strongly correlated with stroke severity. B: Forelimb performance five days after the lesion is not correlated with stroke severity. C: Forelimb performance ten days after the lesion is moderately correlated with stroke severity. D: Forelimb performance twenty days after the lesion is moderately correlated with stroke severity.

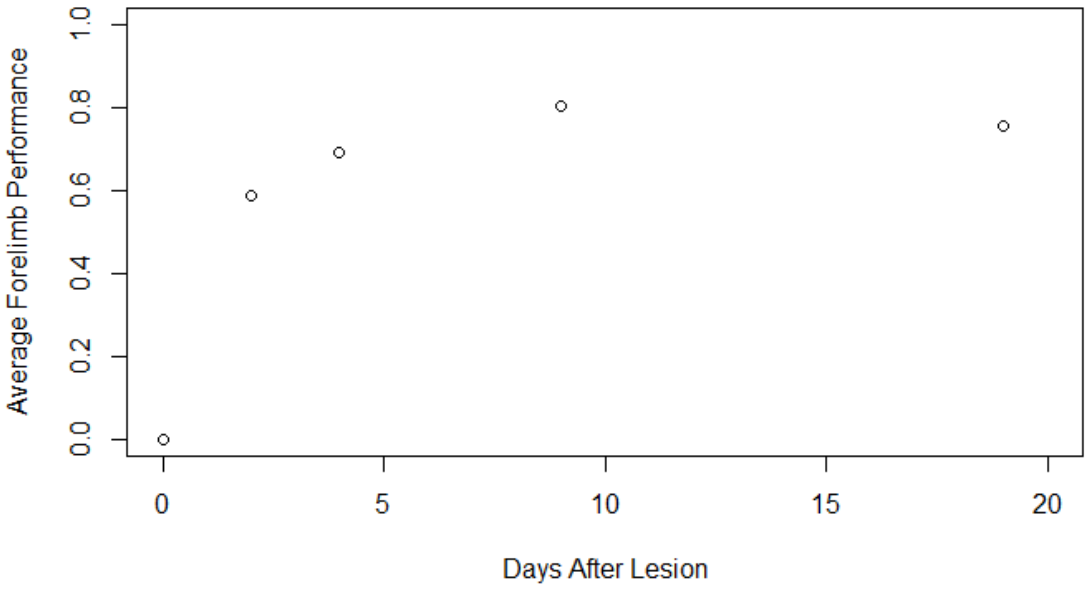

Figure 6: Plot of Stroke Recovery. Mice received cortical lesions or control procedures were allowed 20 days to recover. Forelimb performance was assayed at days 3, 5, 10, and 20 after the lesion. The forelimb performance for this model originates at (0,0) and asymptotically approaches 1 as t increases.

which dictates the rate at which the model approaches 1 (full recovery) as t increases.

Theoretically, this function should appear as a curve originating at $(0, 0)$ and converges to 1, i.e. a full recovery as t increases (see Figure 8). This could be of the form:

$$g(t_j) = \frac{t_j}{t_j + \phi}$$

This would allow us to get $\mathbb{E}[Y]$ at t_j from some function $g(t_j)$ or, equivalently, $g(t_j, \phi)$. Additionally, this function would be true for $\phi \in (0, \infty)$ where ϕ depends on

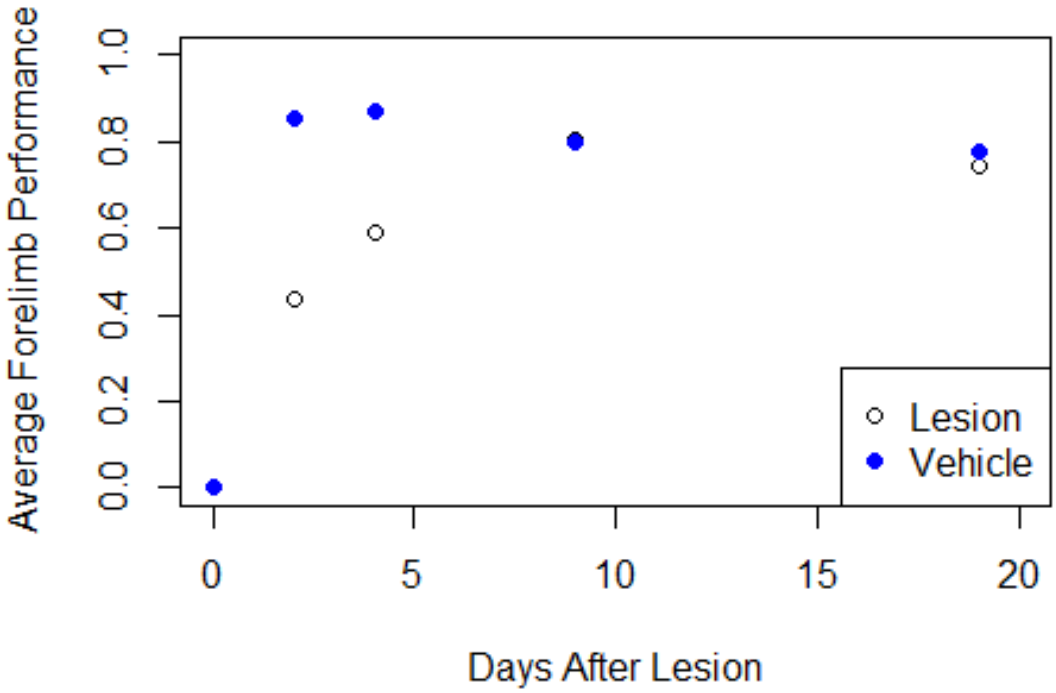

Figure 7: Stroke Recovery by Treatment. Mice that did not receive a lesion approached a full recovery faster than mice that received a lesion. This pattern suggests that the mathematical model for this data should account for subjects with more substantial lesions more slowly approaching a full recovery.

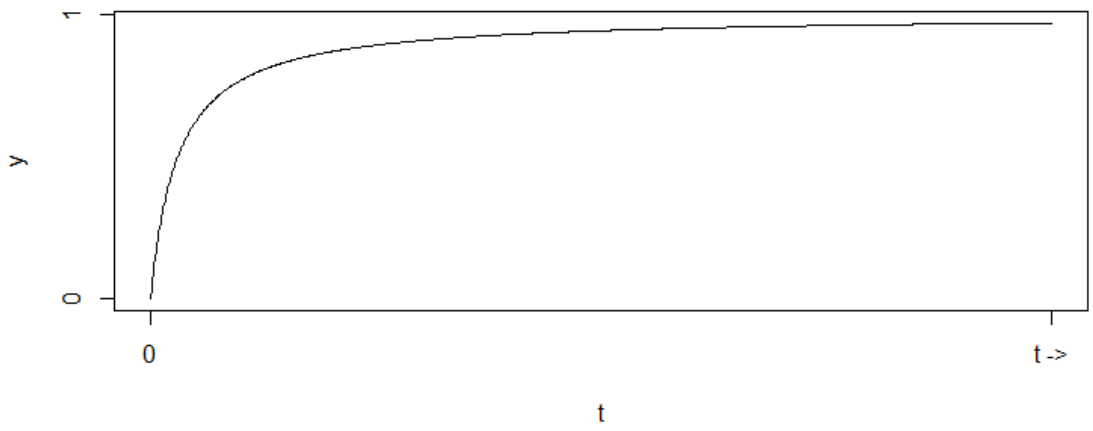

Figure 8: Theoretical Model of Stroke Recovery. Stroke recovery could be understood to originate at (0,0) at the time immediately following the initial event. From here the recovery phase begins and forelimb motor function gets better over time.

x_i or the stroke severity for the ith subject. That is,

$$g(t_j, x_i, \Theta) = \frac{t_j}{t_j + f(x_i, \Theta)}$$

where $f(x_i, \Theta)$ now replaces ϕ but maintains the same properties. That is, just $f(x_i, \theta)$ is a non-decreasing function such that as x_i increases $g(t_j, x_i, \Theta)$ more slowly approaches 1 (see Figure 9).

4.2.1 Non-Linear Model Selection

From the form of the equation for $g(t_j, x_i, \Theta)$ specific $f(x_i, \Theta)$ must be vetted to determine which provides the best fit for the data. In context, stroke severity X_i

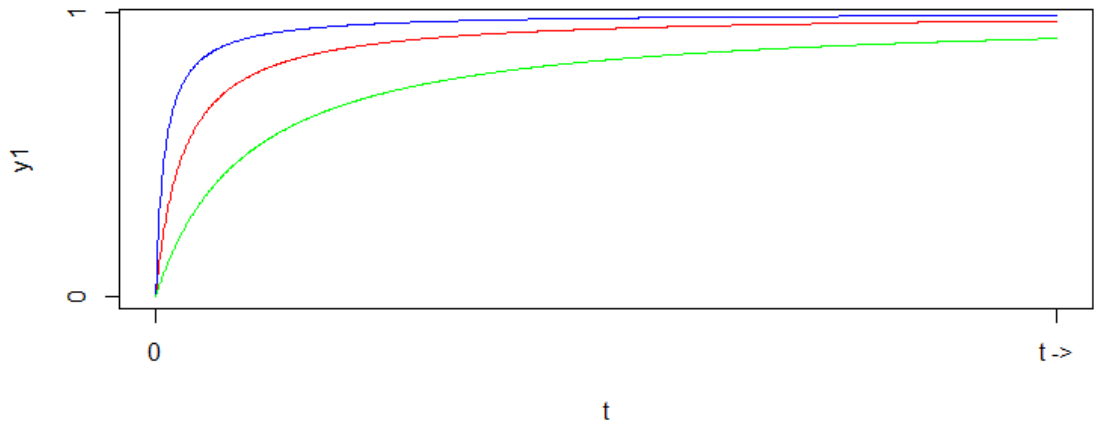

Figure 9: Plot of Function with Varying Convergence Rates. Where the blue line has $\phi = 1$, red line has $\phi = 3$, and green line has $\phi = 20$. This shows that as ϕ increases, the function more slowly approaches 1.

is being used to predict motor function Y_i at time j, or $Y_{i,j}$. Formally, this can be written as:

$$Y_{i,j} = g(t_j, x_i, \Theta) + \sigma\epsilon_{i,j} = \frac{t_j}{t_j + f(x_i, \Theta)} + \sigma\epsilon_{i,j}$$

where $f(x_i, \Theta)$ is a non-decreasing function whose domain is between 0 and ∞ and $\epsilon \sim N(0, \sigma^2)$. We are going to say $\Theta \in \{\theta_1, \theta_2\}$ or Θ is a vector containing two parameters θ_1 and θ_2. In theory, there could be a multitude of parameters contained within Θ but because the dataset is so small, we are just going to limit our search to finding two parameters. Said explicitly,

$$f(x_i, \Theta) = f(x_i, \theta_1, \theta_2)$$

$f(x_i, \theta_1, \theta_2)$	$min \sum_{i=1}^{n} (Y_{i,j} - \frac{t_j}{t_j + f(x_i, \theta_1, \theta_2)})^2$
$X_i\theta_1 + X_i^2\theta_2$	2.440228
$\lvert X_i\rvert\theta_1 + X_i^2\theta_2$	2.716871
$e^{X_i\theta_1} + X_i^2\theta_2$	1.835454
$e^{\lvert X_i\rvert\theta_1} + X_i^2\theta_2$	2.566655
$e^{X_i\theta_1 + X_i^2\theta_2}$	1.932458
$e^{\lvert X_i\rvert\theta_1 + X_i^2\theta_2}$	2.65207
$X_i\theta_1 + e^{X_i^2\theta_2}$	1.932543
$\lvert X_i\rvert\theta_1 + e^{X_i^2\theta_2}$	2.650345

Figure 10: Table of Non-Linear Models and Their Squared Residuals. From this step, the model which has the smallest squared errors was $e^{X_i\theta_1} + X_i^2\theta_2$ which was used to build a hierarchical model and inform the prior that was selected.

When plotting $\bar{Y_j}$ (See Figure 4), where $Y_{i,j}$ is the average of Y_i's at each time point j, against each time point j we get something looks like it could follow the function defined above.

Once determining the general form of our model, a variety of $f(x_i, \theta_1, \theta_2)$ were tested by determining which model resulted in the least amount of error. Stated mathematically, $\hat{\theta_1}$ and $\hat{\theta_2}$ that satisfies

$$\min \sum_{i=1}^{n} \Big(Y_{i,j} - \frac{t_j}{t_j + f(x_i, \theta_1, \theta_2)}\Big)^2$$

and the models were compared based on their sum of squared residuals.

The different forms and corresponding residuals for the non-decreasing $f(x_i, \theta_1, \theta_2) \in (0, \infty)$ constructed are listed in Figure 10.

From this process, the $f(X, \theta_1, \theta_2)$ that produced the smallest squared residuals

which is $e^{X_i\theta_1} + X_i^2\theta_2$ where $\theta_1 = -1.812453$ and $\theta_2 = -0.903245$. When combined with the earlier model of $Y_{i,j}$:

$$Y_{i,j} = g(t_{i,j}, x_i, \Theta) + \sigma\epsilon_{i,j} = \frac{t_{i,j}}{t_{i,j} + f(x_{i,j}, \Theta)} + \sigma\epsilon_{i,j} = \frac{t_{i,j}}{t_{i,j} + e^{X_i\theta_1} + X_i^2\theta_2} + \sigma\epsilon_{i,j}$$

4.2.2 Hierarchical Non-Linear Model

One issue with the previous approach was that the model was constructed by minimizing residuals with respect to mean values of Y_i at each time point t_j. One approach to increase precision with modeling would be to allow each ith subject to have their own θ_1 and θ_2. This approach to statistical modeling is called hierarchical modeling because of the added layer of randomness (a hierarchy). As such, the model for $Y_{i,j}$ will now be constructed via θ_{1i} and θ_{2i}.

$$Y_{i,j} = \frac{t_{i,j}}{t_{i,j} + f(x_i, \theta_{1i}, \theta_{2i})} + \sigma\epsilon_{i,j} = g(t_{i,j}, x_i, \Theta) + \sigma\epsilon_{i,j}$$

To construct a hierarchical model, the $f(x_i, \theta_1, \theta_2)$ from section 4.2.1 will be used. Similarly, $\hat{\theta_{1i}}$ and $\hat{\theta_{2i}}$ for each of the i th subjects which minimizes

$$\min \sum_{i=1}^{n} (Y_{i,j} - \frac{t_j}{t_j + f(x_i, \theta_1, \theta_2)})^2$$

While this model allows for a better fit to the data, the ability to make easy inferences on $\hat{\theta}_{1i}$ and $\hat{\theta}_{2i}$ is lost. The problem is that while by minimizing precision with

$f(x_i, \Theta)$	$\min \sum_{i=1}^{n} \left(Y_{i,j} - \frac{t_j}{t_j + f(x_i, \Theta)}\right)^2$
$f(x_i, \theta_1, \theta_2)$	1.835454
$f(x_i, \theta_{1i}, \theta_{2i})$	1.121639

Figure 11: Comparison of the Non-Linear Model and the Hierarchical Non-Linear Model. By allowing each ith subject to have their own $\hat{\theta}_{1i}$ and $\hat{\theta}_{2i}$ the error in the model was decreased when compared to fixing $\hat{\theta}_1$ and $\hat{\theta}_2$ for each subject.

Subject (i)	$\hat{\theta}_{1i}$	$\hat{\theta}_{2i}$
1	-0.9131514	-1.1715913
2	-1.1514640	-1.0751299
3	-2.5582039	-0.8003722
4	-2.7319317	-0.8168174
5	-2.7281856	-0.8010580
6	-2.9374969	-0.7705752
7	-1.4756275	-0.9587364
8	0.3353608	-1.6042141
9	-1.8650912	-1.0671383
10	1.5408317	0.7647209
11	-0.7370449	-1.2155912

Figure 12: Parameter estimates for the Hierarchical Non-Linear This table shows the $\hat{\theta}_{1i}$ and $\hat{\theta}_{2i}$ for each of the ith subjects.

our estimates, we lose power because the parameter estimates for each ith subject comes from 4 observations. To allow for reliable inferences on these parameters a Bayesian framework will be used where, instead of making inferences on the likelihood estimates (done here), we will make inferences on a posterior distribution (approximated as the product of the likelihood function and a prior distribution).

4.2.3 Bayesian Hierarchical Non-Linear Model

To allow for more power with our parameter estimates, a Bayesian framework can be used to make inferences on a probability distribution which integrates information from the data and prior knowledge. Namely, where previously Θ was estimated by minimizing

$$\sum_{i=1}^{n}\left(Y_{i,j}-\frac{t_j}{t_j+f(x_i,\theta_1,\theta_2)}\right)^2$$

, the assumption was that the data tell everything about estimating Θ that is needed. This is equivalent to maximum likelihood estimation where $l(\theta)=\prod_{i=1}^{n} f(x_i|\theta)$. For example, with our normal model:

$$l(\theta)=\prod_{i=1}^{n}\frac{1}{\sigma\sqrt{2\pi}}e^{-\frac{(x_i-\theta)^2}{2\sigma^2}}$$

From this, when considering that

$$\prod_{i=1}^{n} exp\Big\{-\frac{(x_i-\theta)^2}{2\sigma^2}\Big\}=exp\Big\{-\sum_{i=1}^{n}\frac{(x_i-\theta)^2}{2\sigma^2}\Big\}$$

it can be seen that finding θ by minimizing $\sum_{i=1}^{n}(x_i-\theta)^2$ is equivalent to maximizing the $l(\theta)$. Using this likelihood function is essential to drawing inferences on the parameters from the hierarchical model because it can be used as the vehicle for combining information from the data on θ with prior information on θ. Said plainly, Bayesian modeling allows a model to integrate information from more than just the data to

provide estimates on θ. Stated mathematically, θ will now be approximated from a posterior distribution of the form:

$$\pi_n(\theta) \propto l(\theta)\pi(\theta)$$

Where $\pi_n(\theta)$ is our posterior distribution for θ. To get the Bayes estimator for θ an integral must be evaluated $I = \int \theta\pi_n(\theta)d\theta$. This integral is rather cumbersome to do by hand so simulation can be used where $\theta_1, ..., \theta_M$ are pulled from $\pi_n(\theta)$ and used to estimate I using $\frac{1}{M}\sum_{m=1}^{M}\theta_m$.

To get Bayesian estimates for θ_{1i} and θ_{2i}, a posterior distribution for each of the Θ_i was constructed and Monte Carlo simulation was used to get $\hat{\Theta}_i$. As a reminder, the hierarchical non-linear model constructed is:

$$Y_{i,j} = \frac{t_{i,j}}{t_{i,j} + f(x_i, \theta_{1i}, \theta_{2i})} + \sigma\epsilon_{i,j}$$

where $\epsilon_{i,j} \sim N(0, \sigma^2)$ which can be re-written as

$$Y_{i,j} \sim N\left(\frac{t_{i,j}}{t_{i,j} + f(x_i, \theta_{1i}, \theta_{2i})}, \sigma^2\right)$$

. From this, the likelihood function can be constructed:

$$l(\Theta_i) = \prod_{j=1}^{k} \frac{1}{\sigma\sqrt{2\pi}} exp\left\{\left(- \frac{Y_{i,j} - \frac{t_{i,j}}{t_{i,j}+f(x_i,\theta_{1i},\theta_{2i})}}{\sigma}\right)^2\right\}$$

As the focus is in estimating θ_{1i} and θ_{2i}, σ^2 was set as a constant. Specifically, σ^2 was set to

$$\hat{\sigma}^2 = \frac{\sum_{j=1}^{m}\sum_{i=1}^{n}(Y_{i,j} - \frac{t_j}{t_j + f(x_i,\Theta)})^2}{nm}$$

The prior was constructed by using the NLM selected in 4.2.1 to provide good estimates on where θ_{1i} and θ_{2i} arise. Stated mathematically,

$$\pi(\theta) \sim N\left(\begin{pmatrix}\hat{\theta}_1 \\ \hat{\theta}_2\end{pmatrix}, \Sigma\right)$$

where $\hat{\theta_1}$ and $\hat{\theta_2}$ were estimated from $f(x_i, \theta_1, \theta_2)$. Furthermore:

$$\Sigma = \begin{bmatrix}\tau_1^2 & 0 \\ 0 & \tau_2^2\end{bmatrix}$$

where τ_1^2 and τ_2^2 were estimated such that $\pm 2\tau_1 = 2.8$ and $\pm 2\tau_2 = 2.8$

To get the Bayesian estimates for θ_{1i} and θ_{2i}, the posterior distribution must be constructed which will be of the form: $\pi_n(\theta) \propto l(\theta)\pi(\theta)$.

$$\pi_n(\theta_{1i}, \theta_{2i}|data) \propto exp\left\{ -\frac{1}{2}\sum_{j=1}^{k}\left(\frac{Y_{i,j} - g(\theta_{1i}, \theta_{2i}, x_i, t_{i,j})}{\sigma}\right)^2 \right\} N(\Theta_i|\hat{\Theta}, \Sigma)$$

From this equation, to get the Bayesian estimator for $\theta_1 i$ and $\theta_2 i$ the integral $\int \theta\pi_n(\theta)d\theta$ must be solved. To solve this equation, the Bayesian estimator was approximated using the Metropolis-Hastings algorithm where $\theta_1, ..., \theta_M$ are iteratively

pulled from non-stationary proposal densities M times and use $\frac{1}{M}\sum_{m=1}^{M}\theta_m$ for the Bayesian estimates of θ_{1i} and θ_{2i}. A single iteration of the Metropolis-Hastings algorithm starts with pulling an initial Θ_{1i} from a $N(\hat{\Theta}, \Sigma)$. From here, the algorithm

1) Pulls a proposal $\tilde{\Theta}_{2i}$ from a $N(\hat{\Theta}, \Sigma)$.

2) Selects u from $Unif(0, 1)$

3) If $u < l(\tilde{\Theta}_{2i})/l(\Theta_{1i})$, $\Theta_{2i} = \tilde{\Theta}_{2i}$ else $\Theta_{2i} = \Theta_{1i}$.

4) Repeats steps 1-3 M times and uses $\frac{1}{M}\sum_{m=1}^{M}\Theta_m$ as the Bayesian estimates for θ_{1i} and θ_{2i}

From this approach, the Bayesian estimates for $\hat{\Theta}_i$ or $\hat{\theta}_{1i}$ and $\hat{\theta}_{2i}$ were found along with their posterior distributions (see appendix). These estimates were somewhere between the estimates from the NLM and the HNLM. Additionally, the error associated with this model is somewhere between these two models. While some of the variance explained by the model is lost by using the Bayesian approach as opposed to the likelihood approach, more accurate sampling distributions of the parameter estimates (the posterior distribution) are gained.

Subject (i)	NLM $(\hat{\theta}_1, \hat{\theta}_2)$	HNLM $(\hat{\theta}_{1i}, \hat{\theta}_{2i})$	Bayesian HNLM $(\hat{\theta}_{1i}, \hat{\theta}_{2i})$
1	$(-1.812, -0.903)$	$(-0.913, -1.172)$	$(-1.336, -0.996)$
2	$(-1.812, -0.903)$	$(-1.151, -1.075)$	$(-1.375, -0.969)$
3	$(-1.812, -0.903)$	$(-2.558, -0.800)$	$(-2.011, -0.851)$
4	$(-1.812, -0.903)$	$(-2.732, -0.817)$	$(-2.417, -0.810)$
5	$(-1.812, -0.903)$	$(-2.728, -0.801$	$(-2.273, -0.805)$
6	$(-1.812, -0.903)$	$(-2.937, -0.771)$	$(-2.012, -0.863)$
7	$(-1.812, -0.903)$	$(-1.476, -0.959)$	$(-1.778, -0.909)$
8	$(-1.812, -0.903)$	$(0.335, -1.604)$	$(-1.481, -0.965)$
9	$(-1.812, -0.903)$	$(-1.865, -1.067)$	$(-1.862, -0.966)$
10	$(-1.812, -0.903)$	$(1.540, 0.765)$	$(-1.395, -0.580)$
11	$(-1.812, -0.903)$	$(-0.737, -1.216)$	$(-1.536, -0.954)$

Figure 13: Parameter estimates for the NLM, HNLM, and Bayesian HNLM. The Bayesian parameter estimates typically fall between the estimates for the NLM and for the HNLM as they are approximated from a mixture of the two approaches.

5 Discussion

This project aimed to link the time-course recovery of forelimb function neurovascular remodeling following ischemic lesions to the SMC. While it is well established that these events both occur following a stroke, an animal model which allows them to be studied in tandem has not existed. This model became possible because many advances have happened recently which have allowed repeatedly imaging the cortex of mice (Mostany, R, Portera-Cailliau, C, 2008; Yang et al., 2010; Holmaat et al., 2009; Svoboda et al., 1997; Tomita et al., 2005). This study addressed a large shortcoming by using behavioral manipulations with *in vivo* imaging to explore the relationship between motor improvements and recovery of blood flow in peri-infarct cortex. By designing this experiment such that measurements were taken for individual subjects

at multiple timepoints, we aimed to use the data from early after the stroke to model later recovery.

As we were interested in combining in vivo imaging (Kazmi et al., 2013) with sensitive behavioral assays for forelimb motor function (Tennant, Jones, 2009), we developed a mouse model of cortical ischemia with a cranial window installed over the SMC (Holmaat et al., 2009). The mouse as a model was ideal for this study as most in vivo imaging techniques have been developed using mouse models (namely for their thin skulls and transgenic capabilities) (Mostany, Portera-Cailliau, 2008; Yang et al., 2010; Holmaat et al., 2009; Svoboda et al., 1997; Tomita et al., 2005; Kazmi et al., 2013). By imaging cortical blood flow through a chronic cranial window, we using in vivo multi-exposure speckle imaging (MESI) (Kazmi et al., 2013) to track, follow the temporal recovery of cortical blood flow after an ischemic injury. In mice with cranial windows, a photothrombotic infarct was created in the forelimb area of SMC, which is established to result in upper extremity (forelimb) dysfunction (Farr, Whishaw, 2002; Tennant, Jones, 2009). Additionally, focused infarcts to the SMC in rodents has been shown to reliably induce upper extremity impairments (Tennant, Jones, 2009).

Forelimb function was evaluated using the PMRT as it is established as both a reliable metric for skilled forelimb function and as a model of motor rehabilitative training, i.e., it can be used to promote improvements in skilled forelimb function after SMC infarcts (Tennant, Jones, 2009). Photothrombotic lesions were used because this method allows non-invasive infarct induction through cranial windows and minimizes

the potential for other aspects of the induction procedure to disrupt vasculature (Brown et al., 2007; Brown et al., 2009). We used a cranial window installed over the SMC to allow for repeated imaging of cortical blood flow (Kazmi et al., 2013). Creating the lesions over the SMC allowed us to track motor recovery over time and determine the extent to which the blood flow changes following a stroke are temporally linked with recovery in motor function.

Mice displayed decreased forelimb performance for 5 days following the lesion compared to controls. Additionally, blood flow returned to basal levels by 3 days following the stroke. Furthermore, stroke severity is stronly correlated with functional performance 3 days after the stroke. This pattern gives rise to non-linear modeling which becomes necessary with looking at multiple timepoints. This pattern suggests that

Furthermore, non-linear modeling allowed us to make precise predictions on recovery at time point t when a mouse had a stroke severity of x. This modeling was extended so that each mouse had their own recovery trajectory which minimized the overall variance with the model. To get more accurate estimates for the parameters of this hierarchical model, we attached a prior distribution (estimated by the NLM) which provided us with a posterior distribution from which to make inferences on. The drawback is that we lost a little of the explained variance in the modeling.

Our findings demonstrate the predictive capacity for neuro-anatomically relevant damage to behavioral recovery. This mouse model can be used to explore the

influence of behavioral and pharmacological manipulations on the outcome of stroke. Additionally, the statistical models constructed herein can be scaled to further develop diagnostics surrounding stroke.

6 Appendix

6.1 Raw Data

t	y	x	treat	subject	code
-14	4	-0.6208232	1	1	W9
-14	4	-0.7747727	1	2	W28
-14	3	-0.4592380	1	3	W29
-14	3	-0.9307534	1	4	W30
-14	1	-0.6455666	1	5	W40
-14	4	-0.3484653	1	6	W41
-14	1	-0.2333166	1	7	W42
-14	0	-0.3470111	0	9	W1
-14	2	0.7631883	0	10	W34
-14	4	0.4251561	0	11	W35
-14	4	-0.4402295	0	12	W36
-13	7	-0.6208232	1	1	W9
-13	6	-0.7747727	1	2	W28
-13	3	-0.4592380	1	3	W29
-13	5	-0.9307534	1	4	W30
-13	7	-0.6455666	1	5	W40
-13	3	-0.3484653	1	6	W41

t	y	x	treat	subject	code
-13	10	-0.2333166	1	7	W42
-13	5	-0.3470111	0	9	W1
-13	7	0.7631883	0	10	W34
-13	8	0.4251561	0	11	W35
-13	7	-0.4402295	0	12	W36
-12	6	-0.6208232	1	1	W9
-12	7	-0.7747727	1	2	W28
-12	6	-0.4592380	1	3	W29
-12	8	-0.9307534	1	4	W30
-12	7	-0.6455666	1	5	W40
-12	7	-0.3484653	1	6	W41
-12	10	-0.2333166	1	7	W42
-12	5	-0.3470111	0	9	W1
-12	5	0.7631883	0	10	W34
-12	10	0.4251561	0	11	W35
-12	6	-0.4402295	0	12	W36
-11	5	-0.6208232	1	1	W9
-11	8	-0.7747727	1	2	W28
-11	4	-0.4592380	1	3	W29
-11	3	-0.9307534	1	4	W30

t	y	x	treat	subject	code
-11	9	-0.6455666	1	5	W40
-11	10	-0.3484653	1	6	W41
-11	11	-0.2333166	1	7	W42
-11	6	-0.3470111	0	9	W1
-11	11	0.7631883	0	10	W34
-11	5	0.4251561	0	11	W35
-11	6	-0.4402295	0	12	W36
-10	7	-0.6208232	1	1	W9
-10	9	-0.7747727	1	2	W28
-10	5	-0.4592380	1	3	W29
-10	7	-0.9307534	1	4	W30
-10	9	-0.6455666	1	5	W40
-10	11	-0.3484653	1	6	W41
-10	9	-0.2333166	1	7	W42
-10	10	-0.3470111	0	9	W1
-10	9	0.7631883	0	10	W34
-10	9	0.4251561	0	11	W35
-10	9	-0.4402295	0	12	W36
-9	8	-0.6208232	1	1	W9
-9	12	-0.7747727	1	2	W28

t	y	x	treat	subject	code
-9	12	-0.4592380	1	3	W29
-9	10	-0.9307534	1	4	W30
-9	8	-0.6455666	1	5	W40
-9	7	-0.3484653	1	6	W41
-9	6	-0.2333166	1	7	W42
-9	7	-0.3470111	0	9	W1
-9	11	0.7631883	0	10	W34
-9	9	0.4251561	0	11	W35
-9	9	-0.4402295	0	12	W36
-8	5	-0.6208232	1	1	W9
-8	11	-0.7747727	1	2	W28
-8	12	-0.4592380	1	3	W29
-8	8	-0.9307534	1	4	W30
-8	9	-0.6455666	1	5	W40
-8	10	-0.3484653	1	6	W41
-8	11	-0.2333166	1	7	W42
-8	9	-0.3470111	0	9	W1
-8	7	0.7631883	0	10	W34
-8	8	0.4251561	0	11	W35
-8	13	-0.4402295	0	12	W36

t	y	x	treat	subject	code
-7	7	-0.6208232	1	1	W9
-7	11	-0.7747727	1	2	W28
-7	11	-0.4592380	1	3	W29
-7	7	-0.9307534	1	4	W30
-7	8	-0.6455666	1	5	W40
-7	13	-0.3484653	1	6	W41
-7	9	-0.2333166	1	7	W42
-7	13	-0.3470111	0	9	W1
-7	9	0.7631883	0	10	W34
-7	11	0.4251561	0	11	W35
-7	15	-0.4402295	0	12	W36
-6	7	-0.6208232	1	1	W9
-6	5	-0.7747727	1	2	W28
-6	10	-0.4592380	1	3	W29
-6	7	-0.9307534	1	4	W30
-6	5	-0.6455666	1	5	W40
-6	5	-0.3484653	1	6	W41
-6	4	-0.2333166	1	7	W42
-6	11	-0.3470111	0	9	W1
-6	10	0.7631883	0	10	W34

t	y	x	treat	subject	code
-6	11	0.4251561	0	11	W35
-6	9	-0.4402295	0	12	W36
-5	9	-0.6208232	1	1	W9
-5	11	-0.7747727	1	2	W28
-5	13	-0.4592380	1	3	W29
-5	7	-0.9307534	1	4	W30
-5	9	-0.6455666	1	5	W40
-5	13	-0.3484653	1	6	W41
-5	9	-0.2333166	1	7	W42
-5	6	-0.3470111	0	9	W1
-5	8	0.7631883	0	10	W34
-5	8	0.4251561	0	11	W35
-5	8	-0.4402295	0	12	W36
-4	7	-0.6208232	1	1	W9
-4	12	-0.7747727	1	2	W28
-4	12	-0.4592380	1	3	W29
-4	7	-0.9307534	1	4	W30
-4	8	-0.6455666	1	5	W40
-4	9	-0.3484653	1	6	W41
-4	7	-0.2333166	1	7	W42

t	y	x	treat	subject	code
-4	8	-0.3470111	0	9	W1
-4	10	0.7631883	0	10	W34
-4	13	0.4251561	0	11	W35
-4	11	-0.4402295	0	12	W36
-3	7	-0.6208232	1	1	W9
-3	11	-0.7747727	1	2	W28
-3	10	-0.4592380	1	3	W29
-3	8	-0.9307534	1	4	W30
-3	7	-0.6455666	1	5	W40
-3	7	-0.3484653	1	6	W41
-3	7	-0.2333166	1	7	W42
-3	11	-0.3470111	0	9	W1
-3	10	0.7631883	0	10	W34
-3	7	0.4251561	0	11	W35
-3	8	-0.4402295	0	12	W36
-2	6	-0.6208232	1	1	W9
-2	12	-0.7747727	1	2	W28
-2	16	-0.4592380	1	3	W29
-2	13	-0.9307534	1	4	W30
-2	11	-0.6455666	1	5	W40

t	y	x	treat	subject	code
-2	10	-0.3484653	1	6	W41
-2	9	-0.2333166	1	7	W42
-2	10	-0.3470111	0	9	W1
-2	13	0.7631883	0	10	W34
-2	9	0.4251561	0	11	W35
-2	9	-0.4402295	0	12	W36
-1	7	-0.6208232	1	1	W9
-1	8	-0.7747727	1	2	W28
-1	5	-0.4592380	1	3	W29
-1	3	-0.9307534	1	4	W30
-1	14	-0.6455666	1	5	W40
-1	11	-0.3484653	1	6	W41
-1	12	-0.2333166	1	7	W42
-1	9	-0.3470111	0	9	W1
-1	11	0.7631883	0	10	W34
-1	7	0.4251561	0	11	W35
-1	8	-0.4402295	0	12	W36
0	0	-0.6208232	1	1	W9
0	0	-0.7747727	1	2	W28
0	0	-0.4592380	1	3	W29

t	y	x	treat	subject	code
0	0	-0.9307534	1	4	W30
0	0	-0.6455666	1	5	W40
0	0	-0.3484653	1	6	W41
0	0	-0.2333166	1	7	W42
0	0	-0.3470111	0	9	W1
0	0	0.7631883	0	10	W34
0	0	0.4251561	0	11	W35
0	0	-0.4402295	0	12	W36
2	4	-0.6208232	1	1	W9
2	4	-0.7747727	1	2	W28
2	9	-0.4592380	1	3	W29
2	2	-0.9307534	1	4	W30
2	5	-0.6455666	1	5	W40
2	7	-0.3484653	1	6	W41
2	8	-0.2333166	1	7	W42
2	11	-0.3470111	0	9	W1
2	16	0.7631883	0	10	W34
2	8	0.4251561	0	11	W35
2	11	-0.4402295	0	12	W36
4	9	-0.6208232	1	1	W9

t	y	x	treat	subject	code
4	12	-0.7747727	1	2	W28
4	9	-0.4592380	1	3	W29
4	5	-0.9307534	1	4	W30
4	4	-0.6455666	1	5	W40
4	5	-0.3484653	1	6	W41
4	6	-0.2333166	1	7	W42
4	10	-0.3470111	0	9	W1
4	15	0.7631883	0	10	W34
4	10	0.4251561	0	11	W35
4	12	-0.4402295	0	12	W36
9	8	-0.6208232	1	1	W9
9	9	-0.7747727	1	2	W28
9	11	-0.4592380	1	3	W29
9	8	-0.9307534	1	4	W30
9	11	-0.6455666	1	5	W40
9	12	-0.3484653	1	6	W41
9	12	-0.2333166	1	7	W42
9	12	-0.3470111	0	9	W1
9	12	0.7631883	0	10	W34
9	8	0.4251561	0	11	W35

t	y	x	treat	subject	code
9	11	-0.4402295	0	12	W36
19	7	-0.6208232	1	1	W9
19	10	-0.7747727	1	2	W28
19	10	-0.4592380	1	3	W29
19	4	-0.9307534	1	4	W30
19	9	-0.6455666	1	5	W40
19	11	-0.3484653	1	6	W41
19	14	-0.2333166	1	7	W42
19	9	-0.3470111	0	9	W1
19	14	0.7631883	0	10	W34
19	8	0.4251561	0	11	W35
19	11	-0.4402295	0	12	W36

6.2 Posteriors and Lines of Best Fit

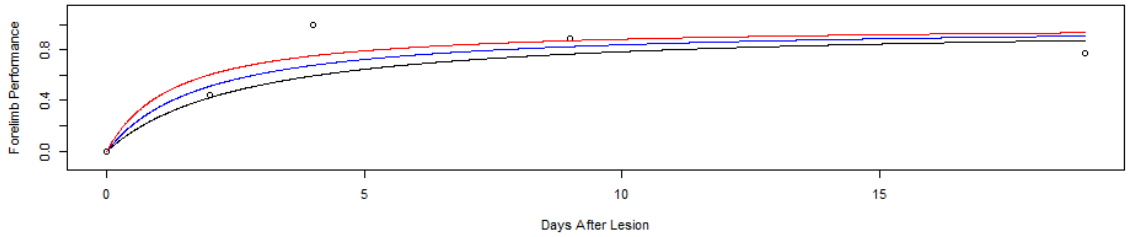

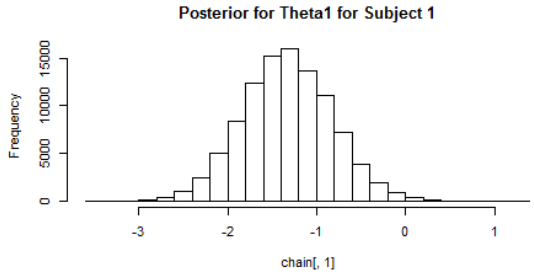

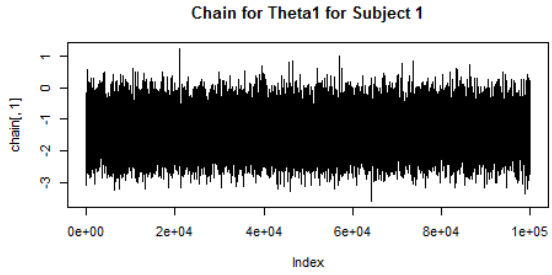

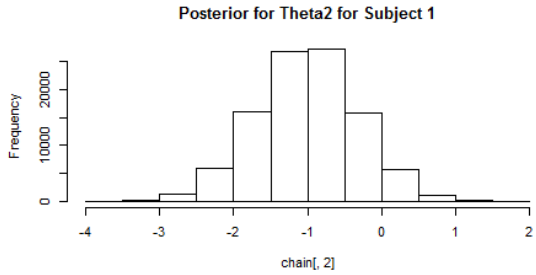

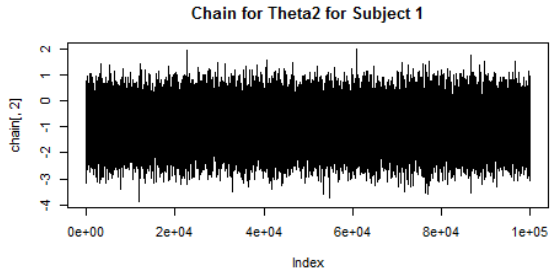

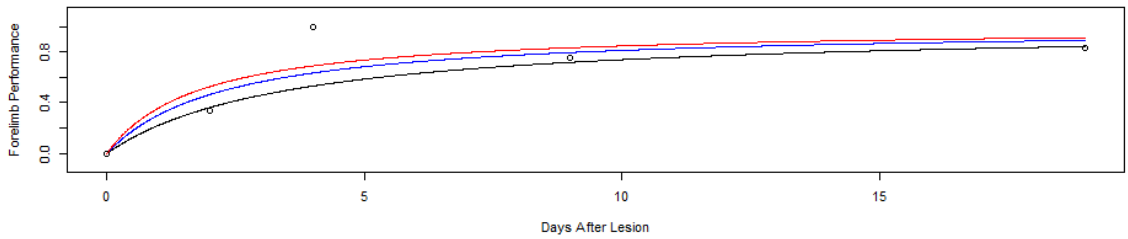
Forelimb Performance
0.0
0.4
0.8
0
5
10
15
Days After Lesion

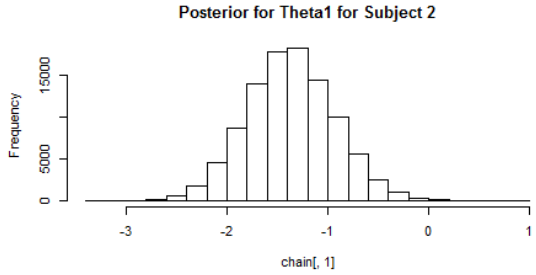
Posterior for Theta1 for Subject 2
Frequency
0
5000
15000
-3
-2
-1
0
1
chain[, 1]

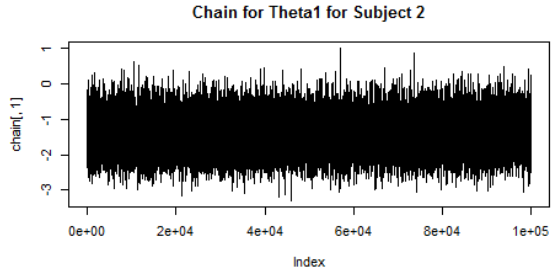
Chain for Theta1 for Subject 2
chain[, 1]
-3
-2
-1
0
1
0e+00
2e+04
4e+04
6e+04
8e+04
1e+05
Index

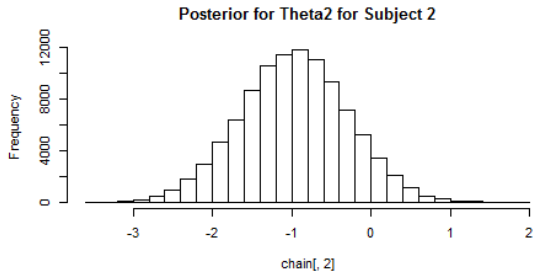
Posterior for Theta2 for Subject 2
Frequency
0
4000
8000
12000
-3
-2
-1
0
1
2
chain[, 2]

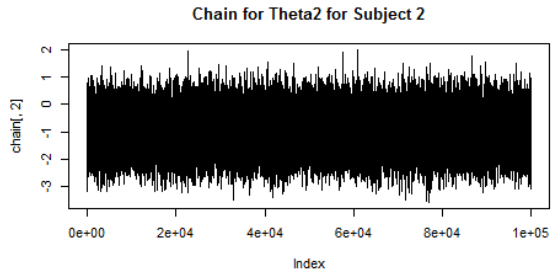
Chain for Theta2 for Subject 2
chain[, 2]
-3
-2
-1
0
1
2
0e+00
2e+04
4e+04
6e+04
8e+04
1e+05
Index

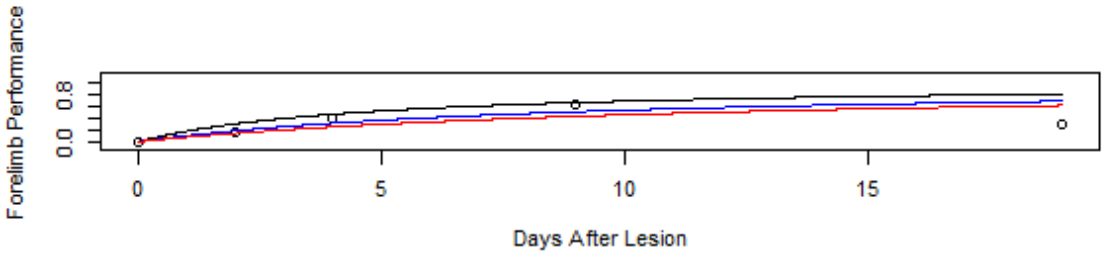
Forelimb Performance
0.0
0.8
0
5
10
15
Days After Lesion

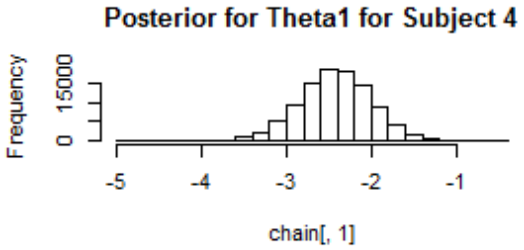
Posterior for Theta1 for Subject 4
Frequency
0
15000
-5
-4
-3
-2
-1
chain[, 1]

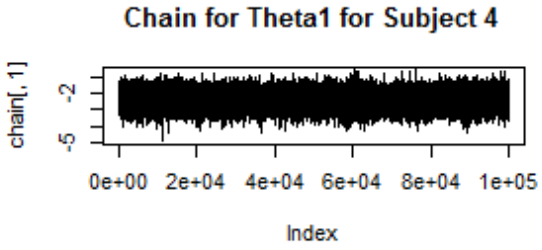
Chain for Theta1 for Subject 4
chain[, 1]
-5
-2
0e+00
2e+04
4e+04
6e+04
8e+04
1e+05
Index

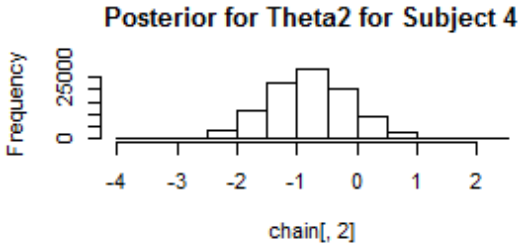
Posterior for Theta2 for Subject 4
Frequency
0
25000
-4
-3
-2
-1
0
1
2
chain[, 2]

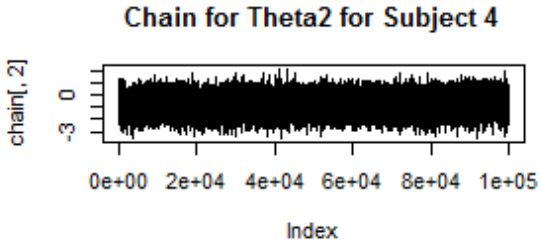
Chain for Theta2 for Subject 4
chain[, 2]
-3
0
0e+00
2e+04
4e+04
6e+04
8e+04
1e+05
Index

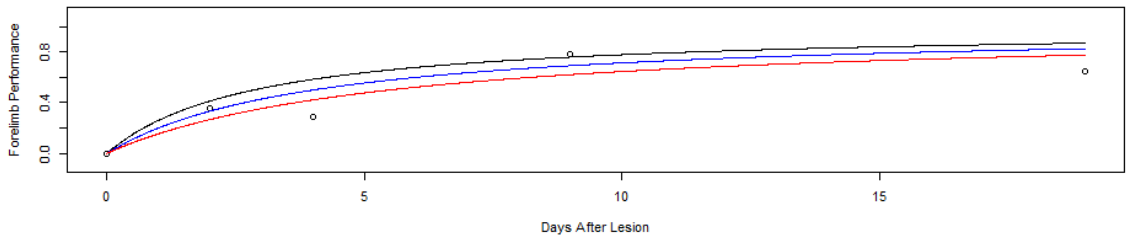
Forelimb Performance
0.0
0.4
0.8
0
5
10
15
Days After Lesion

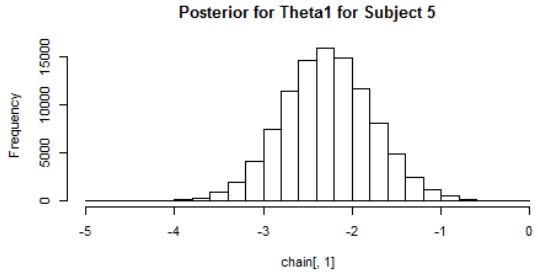
Posterior for Theta1 for Subject 5
Frequency
0
5000
10000
15000
-5
-4
-3
-2
-1
0
chain[, 1]

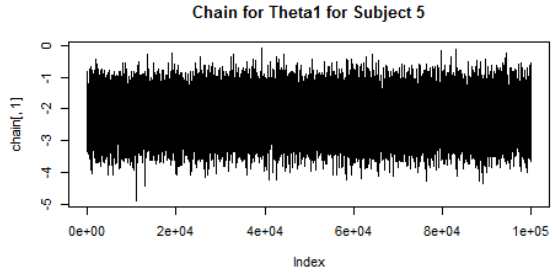
Chain for Theta1 for Subject 5
chain[, 1]
0
-1
-2
-3
-4
-5
0e+00
2e+04
4e+04
6e+04
8e+04
1e+05
Index

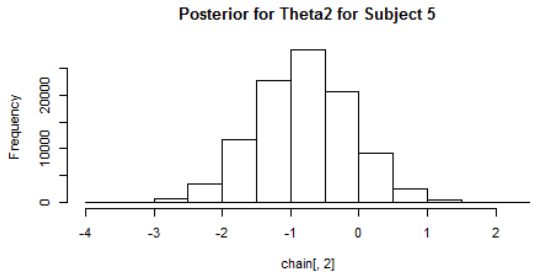
Posterior for Theta2 for Subject 5
Frequency
0
10000
20000
-4
-3
-2
-1
0
1
2
chain[, 2]

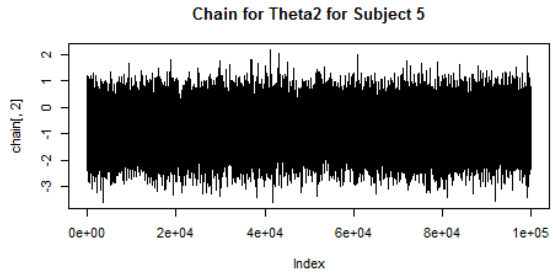
Chain for Theta2 for Subject 5
chain[, 2]
2
1
0
-1
-2
-3
0e+00
2e+04
4e+04
6e+04
8e+04
1e+05
Index

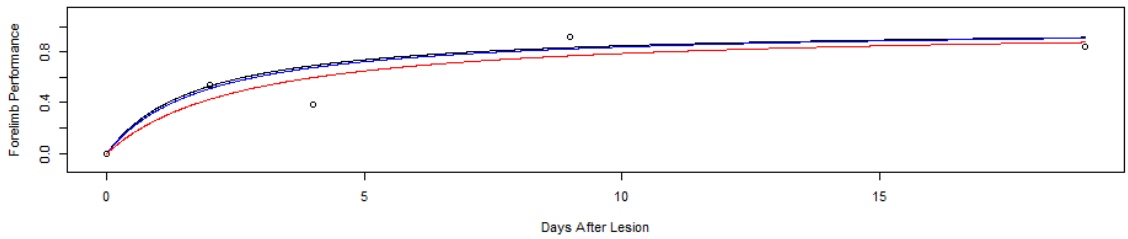
Forelimb Performance
0.0
0.4
0.8
0
5
10
15
Days After Lesion

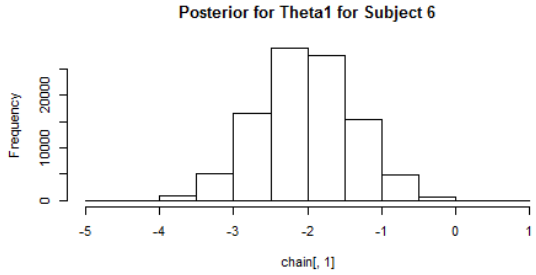
Posterior for Theta1 for Subject 6
Frequency
0
10000
20000
-5
-4
-3
-2
-1
0
1
chain[, 1]

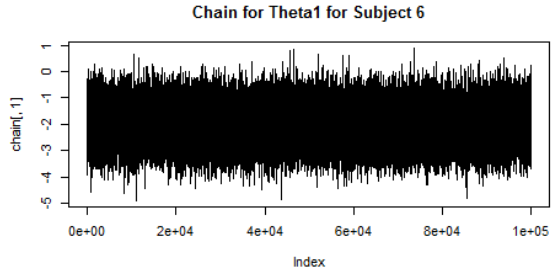
Chain for Theta1 for Subject 6
chain[, 1]
-5
-4
-3
-2
-1
0
1
0e+00
2e+04
4e+04
6e+04
8e+04
1e+05
Index

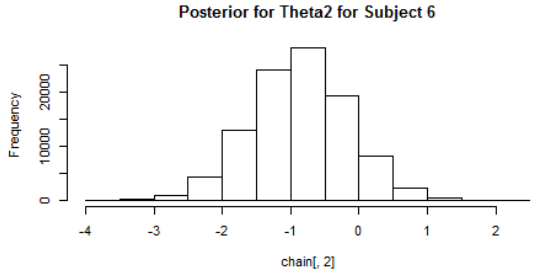
Posterior for Theta2 for Subject 6
Frequency
0
10000
20000
-4
-3
-2
-1
0
1
2
chain[, 2]

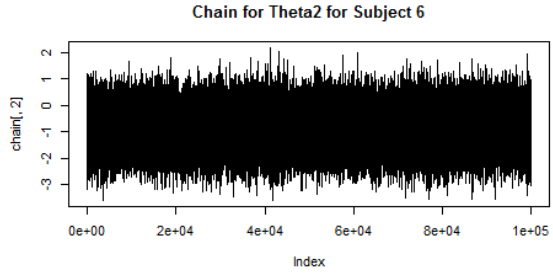
Chain for Theta2 for Subject 6
chain[, 2]
-3
-2
-1
0
1
2
0e+00
2e+04
4e+04
6e+04
8e+04
1e+05
Index

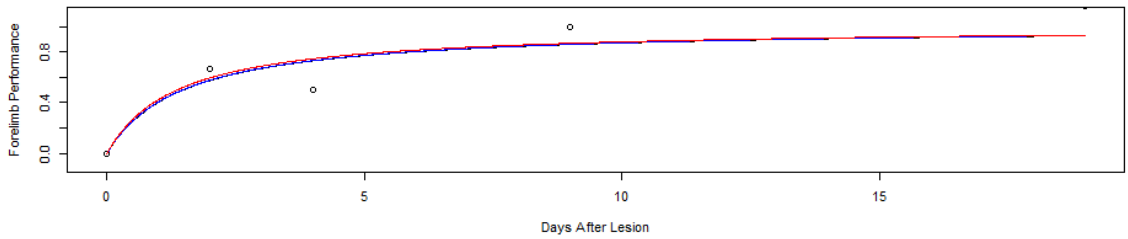
Forelimb Performance
0.0
0.4
0.8
0
5
10
15
Days After Lesion

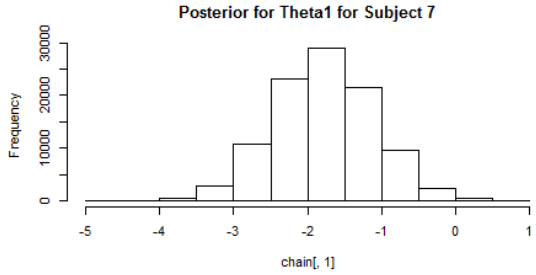
Posterior for Theta1 for Subject 7
Frequency
0
10000
20000
30000
-5
-4
-3
-2
-1
0
1
chain[, 1]

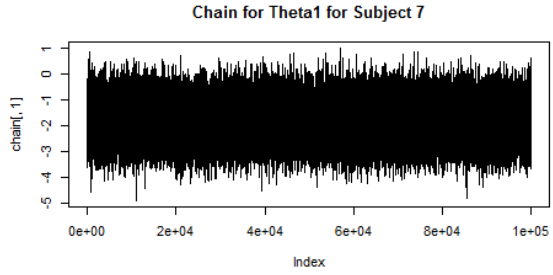
Chain for Theta1 for Subject 7
chain[, 1]
-5
-4
-3
-2
-1
0
1
0e+00
2e+04
4e+04
6e+04
8e+04
1e+05
Index

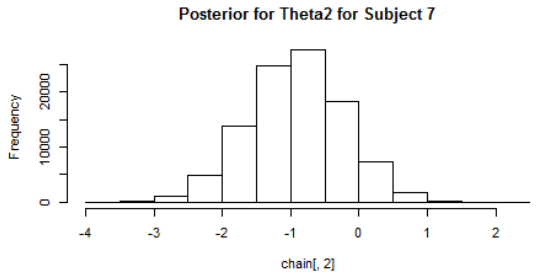
Posterior for Theta2 for Subject 7
Frequency
0
10000
20000
-4
-3
-2
-1
0
1
2
chain[, 2]

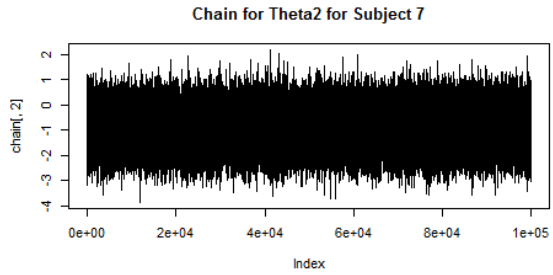
Chain for Theta2 for Subject 7
chain[, 2]
-4
-3
-2
-1
0
1
2
0e+00
2e+04
4e+04
6e+04
8e+04
1e+05
Index

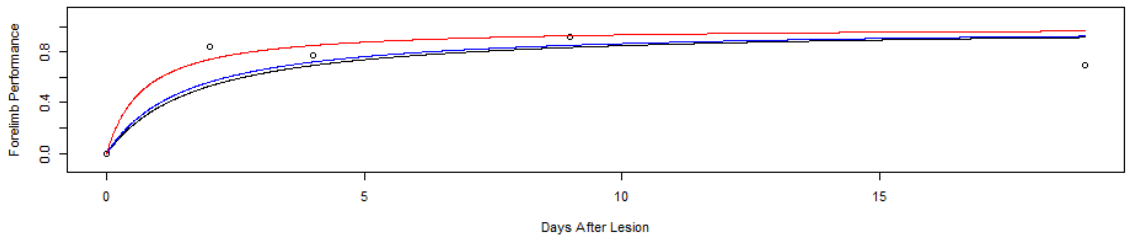
Forelimb Performance
0.0
0.4
0.8
0
5
10
15
Days After Lesion

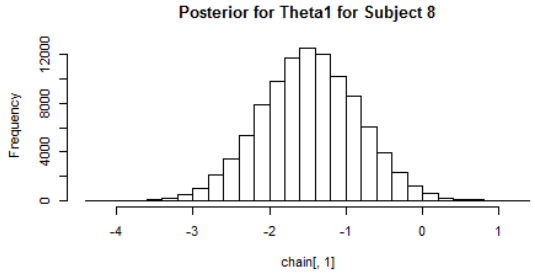
Posterior for Theta1 for Subject 8
Frequency
0
4000
8000
12000
-4
-3
-2
-1
0
1
chain[, 1]

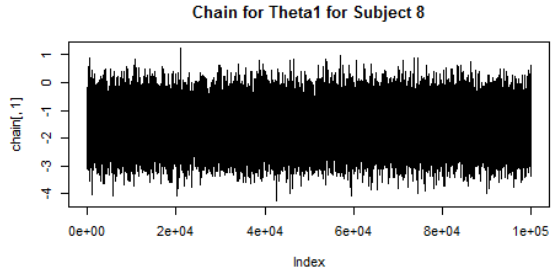
Chain for Theta1 for Subject 8
chain[, 1]
-4
-3
-2
-1
0
1
0e+00
2e+04
4e+04
6e+04
8e+04
1e+05
Index

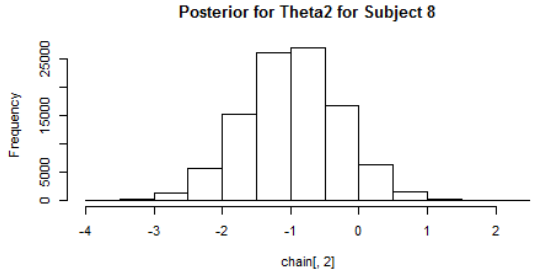
Posterior for Theta2 for Subject 8
Frequency
0
5000
15000
25000
-4
-3
-2
-1
0
1
2
chain[, 2]

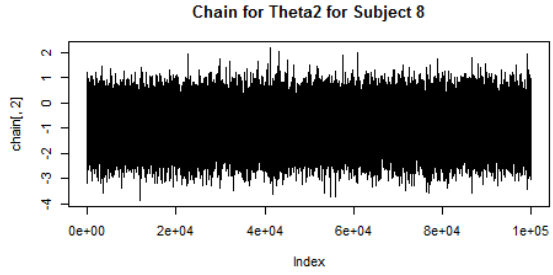
Chain for Theta2 for Subject 8
chain[, 2]
-4
-3
-2
-1
0
1
2
0e+00
2e+04
4e+04
6e+04
8e+04
1e+05
Index

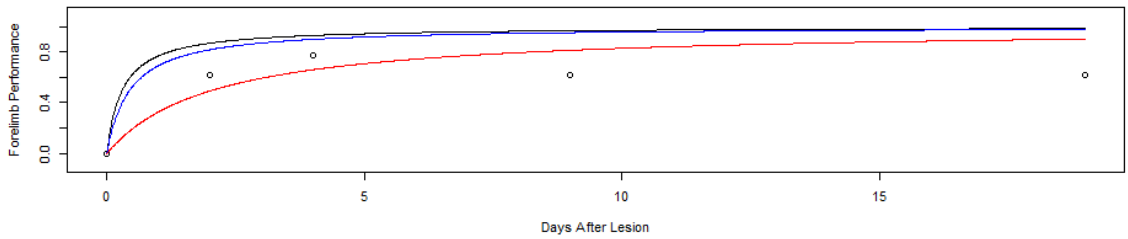
Forelimb Performance
0.0
0.4
0.8
0
5
10
15
Days After Lesion

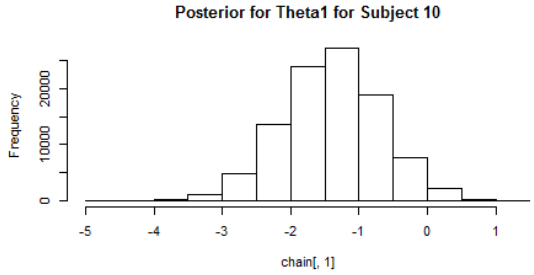
Posterior for Theta1 for Subject 10
Frequency
0
10000
20000
-5
-4
-3
-2
-1
0
1
chain[, 1]

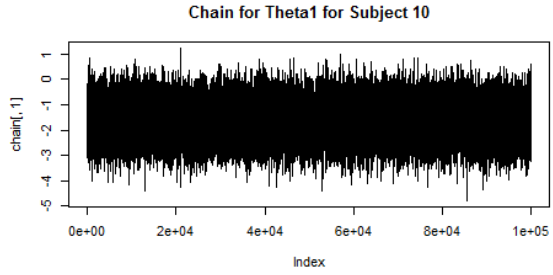
Chain for Theta1 for Subject 10
chain[, 1]
-5
-4
-3
-2
-1
0
1
0e+00
2e+04
4e+04
6e+04
8e+04
1e+05
Index

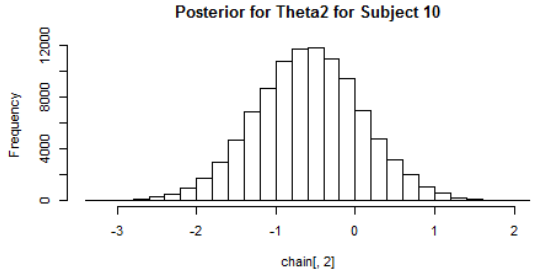
Posterior for Theta2 for Subject 10
Frequency
0
4000
8000
12000
-3
-2
-1
0
1
2
chain[, 2]

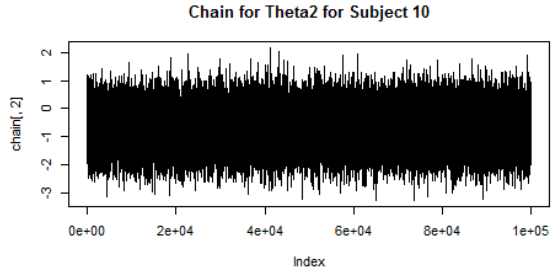
Chain for Theta2 for Subject 10
chain[, 2]
-3
-2
-1
0
1
2
0e+00
2e+04
4e+04
6e+04
8e+04
1e+05
Index

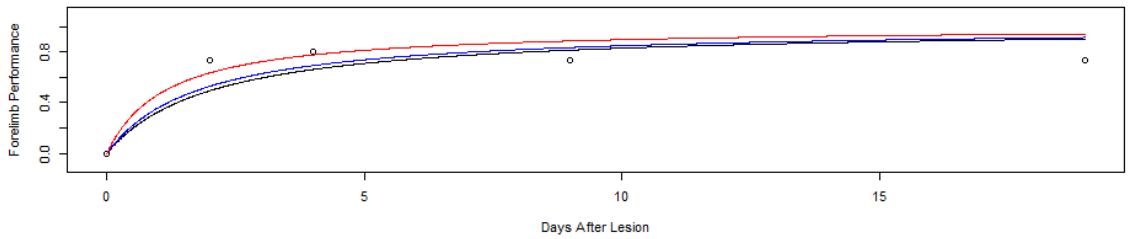
Forelimb Performance
0.0
0.4
0.8
0
5
10
15
Days After Lesion

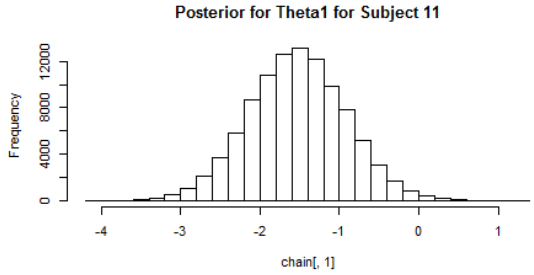
Posterior for Theta1 for Subject 11
Frequency
0
4000
8000
12000
-4
-3
-2
-1
0
1
chain[, 1]

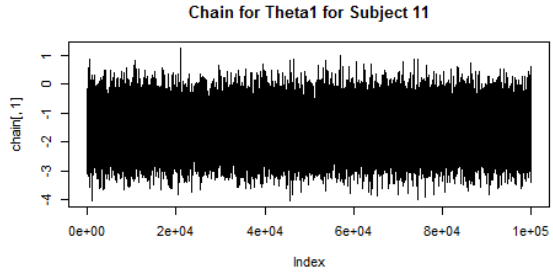
Chain for Theta1 for Subject 11
chain[, 1]
-4
-3
-2
-1
0
1
0e+00
2e+04
4e+04
6e+04
8e+04
1e+05
Index

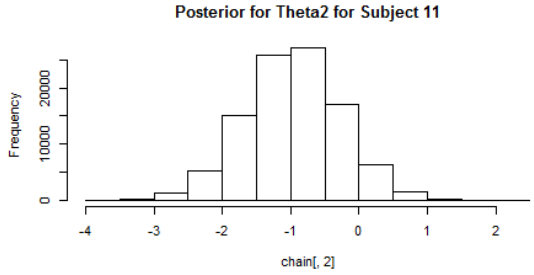
Posterior for Theta2 for Subject 11
Frequency
0
10000
20000
-4
-3
-2
-1
0
1
2
chain[, 2]

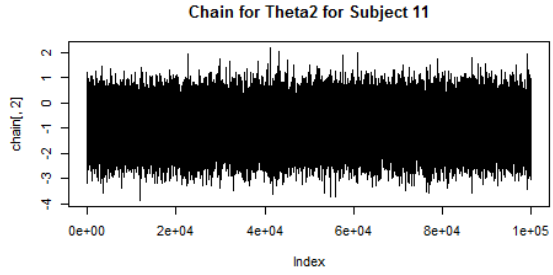
Chain for Theta2 for Subject 11
chain[, 2]
-4
-3
-2
-1
0
1
2
0e+00
2e+04
4e+04
6e+04
8e+04
1e+05
Index

7 References

1. *American Heart Association. Heart Disease and Stroke Statistics: 2013 Update.* (American Heart Association, Dallas, Texas).
2. Lawrence ES, Coshall C, Dundas R, Stewart J, Rudd AG, Howard R, Wolfe CDA. Estimates of the prevalence of acute stroke impairments and disability in a multiethnic population. *Stroke* 32,1279-1284. (2001).
3. Levy CE, Nichols DS, Schmalbrock PM, Keller P, Chakeres DW. Functional MRI evidence of cortical reorganization in upper-limb stroke hemiplegia treated with constraint-induced movement therapy. *Am J Phys Med Rehabil* 80, 4-12 (2001).
4. Liepert et al. Treatment-induced cortical reorganization after stroke in humans. *Stroke* 31, 1210-1216 (2000).
5. Nudo R.J. Adaptive plasticity in motor cortex: implications for rehabilitation after brain injury. *J Rehabil Med*, 7-10 (2003).
6. Taub E, Morris DM. Constraint-induced movement therapy to enhance recovery after stroke. *Curr Atheroscler Rep* 3, 279-286. (2001).
7. Bouet V, Freret T, Toutain J, Divoux D, Boulouard M, Schumann-Bard, P. Sensorimotor and cognitive deficits after transient middle cerebral artery occlusion in the mouse. *Exp. Neurol* 208, 555-567 (2007).
8. Farr TD, Whishaw IQ. Quantitative and qualitative impairments in skilled reaching in the mouse (Mus musculus) after a focal motor cortex stroke. *Stroke*

33, 1869-1875. (2002).

9. Tennant, KA, Jones, TA. Sensorimotor behavioral effects of endothelin-1 induced small cortical infarcts in C57BL/6 mice. *J Neurosci Method* 181, 18-26 (2009).
10. Nudo RJ. Postinfarct cortical plasticity and behavioral recovery. Stroke 38, 840-845 (2007).
11. Biernaskie, J, Corbett, D. Enriched rehabilitative training promotes improved forelimb motor function and enhanced dendritic growth after focal ischemic injury. *J Neurosci* 21, 5272-5280 (2001).
12. Castro-Almancos MA, Borrel J. Functional recovery of forelimb response capacity after forelimb primary motor cortex damage in the rat is due to the reorganization of adjacent areas of cortex. *Neuroscience* 68, 793-805 (1995).
13. Mostany R, Portera-Cailliau C. A craniotomy surgery procedure for chronic brain imaging. *JOVE*. doi.10.3791/680 (2008).
14. Yang G, Pan F, Parkhurst CN, Grutzendler J, Gan WB. Thinned-skull cranial window technique for long-term imaging of the cortex in live mice. Nature Protocols 5, 213-220.
15. Holmaat, A et al. Long-term, high-resolution imaging in the mouse neocortex through a chronic cranial window. *Nature Protocols* 4, 1128-1144 (2009).
16. Svoboda K, Denk W, Kleinfield D, Tank DW. In vivo dendritic calcium dynamics in neocortical pyramidal neurons. *Nature* 85, 161-165 (1997).
17. Tomita et al. Long-term in vivo investigation of mouse cerebral microcirculation

by fluorescence confocal microscopy in the area of focal ischemia. *J Cereb Bld Flow Metab* 25, 858-876 (2005).

18. Kazmi SMS, Parthasarthy A, Song N, Jones TA, Dunn AK. (2013) Chronic imaging of cortical blood flow using multi-exposure speckle imaging. *Journal of Cerebral Blood Flow and Metabolism*, 33:798-808.
19. Biernaskie J, Chernenko G, Corbett D. Efficacy of rehabilitative experience declines with time after focal ischemic brain injury. *J Neurosci* 24, 1245-1254 (2004).
20. Nudo RJ, Wise BM, SiFuentes F, Milliken GW. Neural substrates for the effects of rehabilitative training on motor recovery after ischemic infarct. *Science* 272 1791-1794 (1996).
21. Barbay S, et al. Behaivoral and neurophysiological effects of delayed training following a small ischemic infarct in primary motor cortex of squirrel monkeys. *Exp Brain Res* 169, 106-116 (2005).
22. Xu et al. Rapid formation and selective stabilization of synapses for enduring motor memories. *Nature* 462, 915-920 (2009).
23. Brown, CE, Li, P, Boyd, JD, Delaney, KR, Murphy, TH. Extensive turnover of dendritic spines and vascular remodeling in cortical tissues recovering from stroke. *J Neurosci* 27, 4101-4109 (2007).
24. Brown CE, Aminoltejarl K, Erb H, Winship IR, Murphy TH. In vivo-sensitive dye imaging in adult mice reveals that somatosensory maps lost to stroke are

replaced over weeks by new structural and functional circuits with prolonged modes of activation within both the peri-infarct zone and distant sites. *J Neurosci* 29, 1719-1734 (2009).

25. Mostany R, Chowdhury TG, Johnston DG, Portonovo SA, Carmichael ST, Portera-Cailliau C. Local hemodynamics dictate long-term dendritic plasticity in peri-infarct cortex. *J Neurosci* 42, 14116-26 (2010).
26. Ances BM, Greenberg JH, Detre JA. Laser Doppler imaging of activation-flow coupling in the rat somatosensory cortex. *NeuroImage* 10, 716-723 (1999).
27. Swain RA, et al. Prolonged exercise induces angiogenesis and increases cerebral blood volume in primary motor cortex of the rat. *Neuroscience* 117, 1037-46 (2003).
28. Wei, L, Erinjeri, JP, Rovainen, CM, Woolsey, TA. Collateral growth and angiogenesis around cortical stroke. *Stroke* 32, 2179-2184 (2001).
29. Dirnagl U, Iadecola C, Moskowitz MA. Pathobiology of ischaemic stroke: an integrated view. *Trends in Neuroscience* 22, 391-397.
30. Kerr AL, Wolke ML, Bell JA, Jones TA. Post-stroke protection from maladaptive effects of learning with the non-paretic forelimb by bimanual home cage experience in C57BL/6 mice. *Behavioural Brain Research*, 252: 180-187 (2013).
31. Tennant KA, Kerr AL, Adkins DL, Donlan NA, Thomas N, Kleim JA, Jones TA. Age-dependent reorganization of peri-infarct "pre-motor" cortex with rehabilitative training in mice. NeuroRehabilitation and Neural Repair, in revision.

32. Tennant KA, Adkins DL, Scalco MD, Donlan NA, Asay AL, Kleim JA, Jones TA. Skill learning induced plasticity of motor cortical representations is time and age-dependent. *Neurobiol Learn Mem.* 93(3):291-302 (2012).

33. Tennant KA, Asay AL, Allred RP, Ozburn AR, Jones TA (2010) The Vermicelli and Capellini Handling Tests: Simple quantitative measures of dexterous forepaw function in rats and mice. *Journal of Visualized Experiments*, 41: pii. 2076.

34. Tennant KA, Adkins DL, Donlan NA, Asay AL, Thomas N, Kleim JA, Jones TA (2011) The organization of the forelimb representation of the C57BL/6 mouse motor cortex as defined by intracortical microstimulation and cytoarchitecture. Cerebral Cortex, 21: 865-876.58.

35. Mouton PR, Gokhale AM, Ward NL, West MJ. Stereological length estimation using spherical probes. *J Microsc.* 2002 Apr;206(Pt 1):54-64.

36. Kerr AL, Steuer EL, Pochtarev V, Swain RA. Angiogenesis but not neurogeneis is critical for normal learning and memory. *Neuroscience* 171, 214-226 (2010).

37. Adams RH, Eichmann, A. Axon guidance molecules in vascular patterning. *Cold Spring Harb Perspect Biol.* 2(5):a001985 (2010).

38. Arese M, Serini G, Bussolino F. Nervous vascular parallels; axon guidance and beyond. *Int J Dev Biol.* (4-5):439-445 (2011).

39. Ribatti D. Endogenous inhibitors of angiogenesis: a historical review. *Leuk Res.* 33(5):638-644 (2009).

40. Ohab JJ, Fleming S, Blesch A, Carmichael ST. A neurovascular niche for

neurogenesis after stroke. J Neurosci. Dec 13 2006;26(50):13007-13016.

41. Dobyansky M, Galiano RD, Cetrulo CL, Jr., et al. Endostatin inhibits ischemia-induced neovascularization and increases ischemic tissue loss. Ann Plast Surg. 52(5):512-518 (2004).

42. Schmidt NO, et al. Antiangiogenic therapy by local intracerebral microinfusion improves treatment efficiency and survival in an orthotopic human glioblastoma model. *Clin Cancer Res* 10, 1255-1262 (2004).

43. Widenfalk J, Lipson A, Jubran M, et al. Vascular endothelial growth factor improves functional outcome and decreases secondary degeneration in experimental spinal cord contusion injury. *Neuroscience.* 120(4):951-960 (2003).

44. Kerr AL, Steuer EL, Pochtarev V, Swain RA. Angiogenesis but not neurogeneis is critical for normal learning and memory. *Neuroscience* 171, 214-226 (2010).